Society of Medical Education & Research

2025, Volume 5, Issue 2, Page No: 194-222
ISSN: 3108-4834

Archive of International Journal of Cancer and Allied Science

Oncogenic Role of CircIL4R in Colorectal Cancer via Regulation of the PI3K/AKT Signaling and miR-761/TRIM29/PHLPP1 Axis

Marco De Santis[1]*, Lucia Ferraro[2], Paolo Ricci[1]

[1]Department of Medical Oncology, Faculty of Medicine, Sapienza University of Rome, Rome, Italy.
[2]Department of Molecular Oncology, Faculty of Medicine, University of Milan, Milan, Italy.

***E-mail** ✉ marco.desantis@gmail.com

Abstract

An increasing body of research suggests that abnormal circRNA expression contributes significantly to cancer development and progression, including CRC. Despite this, the clinical implications and mechanistic roles of novel circRNAs in CRC have not yet been fully elucidated. Candidate circRNAs associated with colorectal cancer were first screened using computational approaches and subsequently confirmed in patient-derived samples by quantitative real-time PCR and in situ hybridization. Functional and phenotypic analyses were then carried out using both cellular models and animal systems to assess the role of circIL4R in colorectal cancer progression, as well as its association with clinicopathological features. To delineate the molecular basis of circIL4R activity, multiple mechanistic assays, including RNA pull-down, fluorescence in situ hybridization, luciferase-based reporter assays, and ubiquitination experiments, were employed. Elevated levels of circIL4R were observed in colorectal cancer (CRC) cell lines as well as in serum and tissue samples from CRC patients. This upregulation showed a strong positive association with more severe clinicopathological characteristics and unfavorable patient outcomes. In functional studies, circIL4R was shown to enhance migration, CRC cell proliferation, and invasion through activation of the PI3K/AKT signaling pathway. At the molecular level, circIL4R expression is controlled by the transcription factor TFAP2C, and it acts as a sponge for miR-761, thereby increasing TRIM29 levels. Elevated TRIM29 then promotes ubiquitin-dependent degradation of PHLPP1, leading to activation of the PI3K/AKT pathway and ultimately driving CRC tumor progression. These results indicate that elevated circIL4R expression contributes to colorectal cancer progression and highlight its potential utility as a biomarker for disease diagnosis and prognosis, as well as a candidate target for therapeutic intervention in CRC.

Keywords: Colorectal cancer, miR-761, circIL4R, PI3K/AKT pathway, TRIM29

Introduction

Colorectal cancer (CRC) is among the most prevalent malignancies of the gastrointestinal tract and currently ranks as the second most common cause of cancer-associated mortality worldwide [1]. According to the National Comprehensive Cancer Network (NCCN), the standard therapeutic strategy for CRC involves surgical resection in combination with radiotherapy and chemotherapy [2]. Despite notable advances in treatment approaches, clinical outcomes for CRC patients remain suboptimal, largely owing to the aggressive biological behavior of the disease and incomplete understanding of its molecular pathogenesis. Globally, CRC accounts for approximately 880,000 deaths each year [3]. Consequently, elucidating the molecular mechanisms underlying CRC initiation and progression is critically important for improving early diagnosis, therapeutic efficacy, and patient prognosis.

Circular RNAs (circRNAs) represent a recently recognized class of endogenous RNAs characterized by

Access this article online https://smerpub.com/

Received: 01 September 2025; **Accepted:** 16 December 2025

How to cite this article: Santis MD, Ferraro L, Ricci P. Oncogenic Role of CircIL4R in Colorectal Cancer via Regulation of the PI3K/AKT Signaling and miR-761/TRIM29/PHLPP1 Axis. Arch Int J Cancer Allied Sci. 2025;5(2):194-222. https://doi.org/10.51847/vc5UYl30bM

a covalently closed-loop structure formed through noncanonical back-splicing of precursor messenger RNAs [4]. Unlike linear RNAs, circRNAs lack both 5′ caps and 3′ polyadenylated tails, rendering them resistant to exonuclease-mediated degradation and conferring enhanced molecular stability [5]. With the rapid advancement of high-throughput sequencing technologies and bioinformatics tools, growing evidence has demonstrated that circRNAs are abundantly expressed, evolutionarily conserved, structurally stable, and often exhibit tissue- or cell-type specificity in human malignancies, including CRC [6, 7]. Several circRNAs, such as ciRS-7-A, circNSUN2, and circ-ERBIN, have been reported to be highly expressed in CRC and to promote tumor progression [8-10]. Functionally, circRNAs can regulate cellular processes by sequestering microRNAs (miRNAs), binding to RNA-binding proteins (RBPs), or, in certain cases, serving as templates for protein translation or modulators of transcription and RNA splicing [11-13]. Dysregulated circRNAs have also been implicated in cancer development through modulation of multiple oncogenic signaling pathways, including WNT/β-catenin, MAPK, JAK/STAT, NOTCH, and PI3K/AKT signaling cascades [14, 15]. For instance, Zhang *et al*. reported that hsa_circ_0026628 accelerates CRC progression by targeting SP1 and activating the Wnt/β-catenin pathway [16], while Zheng *et al*. demonstrated that circPPP1R12A facilitates colon cancer metastasis through Hippo-YAP pathway activation [17]. Collectively, these findings highlight circRNAs as promising biomarkers for CRC diagnosis and prognosis, as well as potential therapeutic targets and key regulators of cancer-related signaling networks [18]. TRIM29, also referred to as ATDC, belongs to the tripartite motif-containing protein family and has been shown to exert tumor-promoting effects in multiple cancer types, including pancreatic, thyroid, bladder, and colorectal cancers [19-24]. Previous studies by Han *et al* and Sun *et al*.. revealed that TRIM29 is significantly upregulated in CRC and contributes to malignant progression [22, 23]. Additionally, Xu *et al*. demonstrated that increased TRIM29 expression drives thyroid cancer progression through activation of the PI3K/AKT signaling pathway [24]. Recent research has increasingly emphasized the role of circRNAs in regulating tumorigenesis and cancer progression by modulating the expression of downstream target genes [9, 10]. Therefore, exploring the regulatory relationship between circRNAs and TRIM29 is essential for understanding upstream control mechanisms of TRIM29 and for identifying novel therapeutic strategies for CRC. In recent years, extensive efforts have been made to characterize aberrantly expressed circRNAs and their regulatory networks in diverse malignancies. However, research focusing on circRNAs in CRC remains relatively limited, and the expression patterns, clinical relevance, functional roles, and molecular mechanisms of newly identified circRNAs in CRC are still poorly defined. In this study, bioinformatic screening led to the identification of a previously uncharacterized CRC-associated circRNA, hsa_circ_0038718, which originates from exons 3 and 4 of the IL4R gene and is referred to as circIL4R. Prior to this investigation, the expression profile and biological significance of circIL4R in CRC had not been elucidated. Accordingly, in situ hybridization (ISH) and quantitative real-time PCR (qRT–PCR) analyses were initially employed to assess circIL4R expression levels and evaluate its clinical relevance in CRC specimens. Subsequently, both gain- and loss-of-function approaches were applied in cellular and animal models to clarify the functional role and mechanistic contribution of circIL4R to CRC progression. Detailed mechanistic studies, including chromatin immunoprecipitation (ChIP), luciferase reporter assays, and biotin-labeled RNA pull-down experiments, demonstrated that circIL4R transcription is induced by TFAP2C and that circIL4R functions as a competing endogenous RNA by sponging miR-761, thereby increasing TRIM29 expression. Elevated TRIM29 levels were shown to promote ubiquitin-dependent degradation of PHLPP1, resulting in sustained activation of the PI3K/AKT signaling pathway and enhanced proliferative and metastatic capacities of CRC cells. Taken together, these findings indicate that circIL4R represents a potential therapeutic target and novel diagnostic and prognostic biomarker for colorectal cancer.

Materials and Methods

Clinical specimens

A total of 120 matched pairs of colorectal cancer tissues and adjacent noncancerous tissues (ANTs) were obtained from patients who underwent either curative or palliative surgical resection between January 2015 and September 2016. An independent cohort included 50 patients with confirmed CRC, from whom serum samples were collected both prior to and following surgical treatment

during the period from January 2019 to January 2020. Concurrently, serum specimens were collected from 40 healthy individuals and 40 patients newly diagnosed with CRC. Additionally, 179 paired formalin-fixed, paraffin-embedded CRC tissues and matched ANTs were assembled for the construction of tissue microarrays (TMAs).

All enrolled patients were histologically diagnosed with CRC and had not received chemotherapy or radiotherapy before surgery. Tissue samples were obtained by investigators from the Department of General Surgery at the Affiliated Hospital of Xuzhou Medical University, rapidly frozen in liquid nitrogen following surgical removal, and stored at −80 °C until subsequent RNA isolation. This research protocol was approved by the Ethics Committee of the Affiliated Hospital of Xuzhou Medical University (approval number XYFY2020-KL185-01), and written informed consent was obtained from all participants, including patients and healthy controls.

Culture and cell lines

The normal human colorectal epithelial cell line, FHC, was purchased from the American Type Culture Collection (ATCC; Manassas, VA, USA). In contrast, various human colorectal cancer (CRC) cell lines (SW480, SW620, HT29, LoVo, DLD1, and HCT116) were acquired from the Cell Bank of the Chinese Academy of Sciences (Shanghai, China).

Cells were maintained as follows: HT-29 in RPMI 1640 medium (Gibco, USA); SW620 in L-15 medium (Gibco, USA); DLD1, LoVo, and both FHC and SW480 in high-glucose DMEM (Gibco, USA) and HCT116 in McCoy's 5A medium with 10% fetal bovine serum (FBS; Gibco, USA). All cell lines were incubated at 37°C in a 5% CO_2 humidified atmosphere and confirmed to be free of mycoplasma contamination by testing before experimental use.

Cell transfection

Small interfering RNAs (siRNAs) targeting circIL4R (sicircIL4R#2, sicircIL4R#1), TFAP2C (siTFAP2C), TRIM29 (siTRIM29), and PHLPP1 (siPHLPP1), along with negative control siRNA (siCtrl), as well as miR-761 and miR-541-3p mimics and inhibitors with their corresponding controls, were designed and synthesized by Gene Pharma Technology (Shanghai, China). Cells were grown to 30–50% confluence prior to transfection with siRNAs using siLentFect Lipid Reagent (CA, Bio-Rad, USA) following the manufacturer's protocol. For overexpression studies, the full-length coding sequences of TRIM29, circIL4R, TFAP2C, and PHLPP1 were cloned into the pcDNA3.1 vector (Invitrogen, Shanghai, China), with an empty vector serving as the negative control. When cell confluence reached approximately 90%, plasmid transfections were performed using Lipofectamine 2000 (Invitrogen, Shanghai, China) according to the manufacturer's instructions, and transfected cells were collected 48 hours later for downstream analyses.

Lentiviral vectors targeting human circIL4R (sh-circIL4R#2 and sh-circIL4R#1) and nonspecific control lentiviruses (sh-Ctrl) were also obtained from Gene Pharma Technology (Shanghai, China) and transduced into CRC cells following the manufacturer's protocol. Stable circIL4R knockdown cell lines were selected using puromycin and validated by qRT–PCR.

RNA, qRT–PCR and genomic DNA (gDNA) extraction

Nucleic acid purity and concentration were evaluated using a NanoDrop 2000 spectrophotometer (Thermo Fisher Scientific, USA). Genomic DNA (gDNA) from cells and tissues was purified with the FastPure® Tissue/Cell DNA Isolation Mini Kit (Vazyme, Nanjing, China), and total RNA from CRC cell lines and specimens was obtained via RNA Isolater Total RNA Extraction Reagent (Vazyme, Nanjing, China), all in accordance with the manufacturers' instructions. Cytoplasmic and nuclear RNA fractions from CRC cells were separated employing the PARIS™ Kit (Life Technologies, Texas, Austin, USA).

To quantify mRNA and circRNA expression by cDNA and qRT-PCR, was synthesized from RNA with HiScript II Q RT SuperMix (Vazyme, Nanjing, China). Amplification was subsequently performed using ChamQ SYBR qPCR Master Mix (Vazyme, Nanjing, China) on a LightCycler 96 instrument (Roche, Switzerland) with these parameters: 95°C for 30 s initially, then 40 cycles of 60°C for 60 s and 95°C for 10 s, ending with melting curve analysis.

For miRNA detection via qRT-PCR, stem-loop primers were used in conjunction with the miRNA 1st Strand cDNA Synthesis Kit (Vazyme, Nanjing, China) for reverse transcription. The resulting cDNA was amplified with miRNA Universal SYBR qPCR Master Mix (Vazyme, Nanjing, China) on the LightCycler 96 system under the conditions: 95°C for 5 min, followed by 40

cycles of 60°C for 60 s and 95°C for 10 s, and concluding with melting curve analysis.

Expression levels relative to controls were computed via the $2^{-\Delta\Delta CT}$ approach, using GAPDH as the internal control for mRNAs, 18S rRNA for circRNAs, and U6 for miRNAs.

Chromatin immunoprecipitation (ChIP) assay

Chromatin immunoprecipitation (ChIP) experiments were conducted with the EZ ChIP Chromatin Immunoprecipitation Kit (Millipore, Bedford, MA, USA), adhering to the manufacturer's protocol. In brief, approximately 1×10^7 HCT116 cells underwent crosslinking of proteins to DNA by incubation with 1% formaldehyde for 10 minutes at room temperature. Cells were then rinsed in PBS and disrupted using ChIP lysis buffer. The resulting lysates were fragmented into 200–1000 bp DNA pieces via sonication, followed by overnight incubation at 4°C with either anti-TFAP2C antibodies (Proteintech, Chicago, IL, USA) or control IgG for immunoprecipitation.

Immunohistochemistry (IHC)

Subcutaneous tumors harvested from the experiments were fixed in 4% formalin, paraffin-embedded, and cut into 4-μm-thick sections. Immunohistochemistry (IHC) on both tissue microarrays (TMAs) and these subcutaneous tumor sections was carried out using the streptavidin-peroxidase (SP) Kit (Zhongshan Biotech, Beijing, China) according to the previously described standard procedure [25].

Sections were probed with primary antibodies targeting phosphorylated AKT (Cell Signaling Technology, Danvers, MA, USA), Ki-67 (Cell Signaling Technology, Danvers, MA, USA), TFAP2C (Abcam, Cambridge, MA, USA) , TRIM29 (Proteintech, Chicago, IL, USA), and PHLPP1 (Proteintech, Chicago, IL, USA). Stained slides were imaged using an Olympus microscope (Tokyo, Japan).

Statistical analysis

Statistical analyses were conducted using SPSS version 19.0 (IBM, Armonk, NY, USA) and GraphPad Prism 8.0 (La Jolla, CA, USA). All results are expressed as mean ± standard deviation (SD), with two-tailed tests applied throughout. Statistical significance was defined as $P < 0.05$.

Differences between groups were assessed using Student's t-test or one-way ANOVA, as appropriate. Pearson's correlation coefficient was employed for correlation analyses. The diagnostic performance of circIL4R was evaluated through receiver operating characteristic (ROC) curves to determine sensitivity and specificity. Associations between circIL4R expression levels and clinicopathological features in CRC patients were examined via chi-square test. Kaplan–Meier curves with log-rank tests were generated to estimate disease-free survival (DFS) and overall survival (OS). Univariate and multivariate Cox proportional hazards regression analyses were performed to identify independent prognostic factors, including circIL4R and other clinicopathological variables, and to calculate hazard ratios.

Results and Discussion

Characterized in CRC cells and circIL4R is identified

To identify previously unrecognized circRNAs that may promote CRC progression, we analyzed the GEO dataset GSE126094, which contains ten matched pairs of CRC tissues and adjacent normal tissues (ANTs). Applying thresholds of $|\text{fold-change}| \geq 2$ and $P < 0.05$, 59 circRNAs were found to be significantly dysregulated, including 23 upregulated and 36 downregulated transcripts, as shown in the cluster heatmap **(Figure 1a).** From these, fourteen upregulated circRNAs not previously reported in cancer were selected for further validation in CRC cell lines. Among them, hsa_circ_0038718 showed the most pronounced overexpression across HCT116, DLD1, LoVo, SW620, HT29, and SW480 cells compared to normal FHC cells, leading us to prioritize this circRNA for in-depth study **(Figure 1b)**

Annotation from the circBase database indicated that hsa_circ_0038718 originates from exons 3 and 4 of the IL4R gene (Chr16: 27,351,506–27,353,580) and spans 227 nucleotides, and it was therefore designated circIL4R **(Figure 1c).** To experimentally confirm its circular nature, divergent primers were designed to amplify the back-spliced junction of circIL4R, while convergent primers targeted linear IL4R mRNA. PCR using cDNA and genomic DNA from HCT116 and DLD1 cells revealed that circIL4R was detectable only in cDNA, but not in genomic DNA **(Figure 1d).** RNase R treatment further demonstrated that circIL4R resisted exonuclease digestion, whereas linear IL4R transcripts were degraded **(Figure 1e).** In addition, actinomycin D chase experiments showed that circIL4R exhibited greater stability than the corresponding linear IL4R mRNA

(Figure 1f), confirming the presence of a circular transcript in CRC cells.

The cellular distribution of circIL4R was assessed using nuclear-cytoplasmic fractionation and FISH assays, which both indicated that circIL4R is predominantly localized in the cytoplasm **(Figures 1g and 1h)**. Collectively, these findings demonstrate that circIL4R is a stable, cytoplasm-enriched circRNA that is consistently upregulated in CRC and may play an important role in tumor progression.

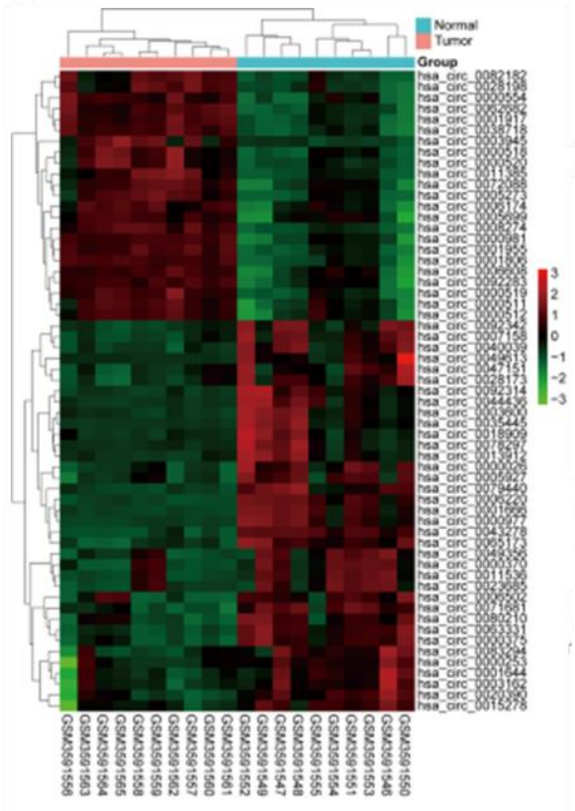

a)

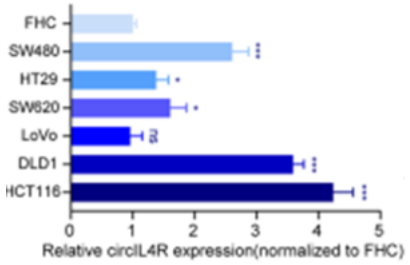

b)

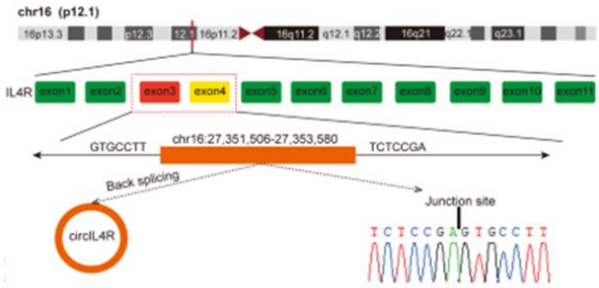

c)

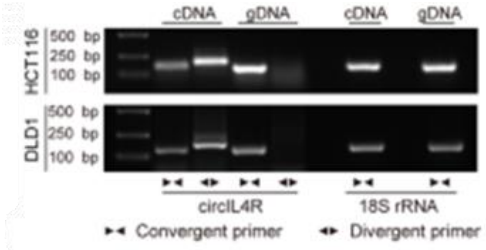

d)

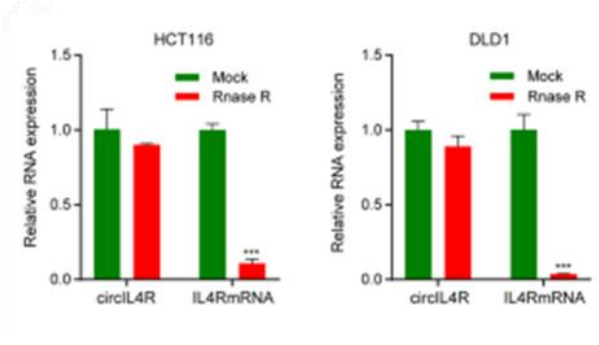

e)

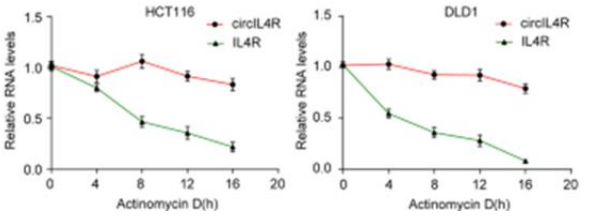

f)

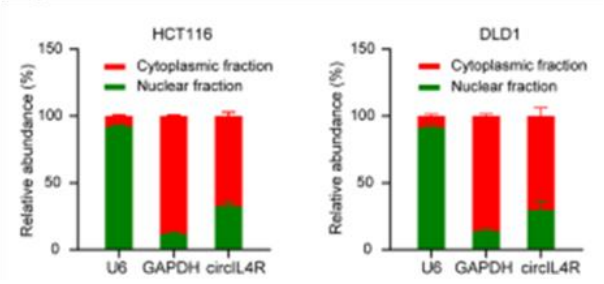

g)

Figure 1. Characterization and identification of circIL4R in colorectal cancer cells. (a) Heatmap

illustrating circRNAs that are differentially expressed in ten CRC tissue samples and their matched adjacent normal tissues (n = 20). Upregulated circRNAs are highlighted in red, and downregulated circRNAs are shown in green. (b) Expression levels of circIL4R in the normal colorectal epithelial cell line FHC and six CRC cell lines (DLD1, HCT116, SW620, LoVo, SW480 and HT29), with 18S rRNA used as the internal reference. (c) Diagram showing circIL4R formation via back-splicing of exons 3 and 4 of the IL4R gene. (d) Agarose gel electrophoresis of PCR products confirmed circIL4R presence: divergent primers amplified circIL4R from cDNA but not from genomic DNA (gDNA); 18S rRNA served as a positive control. (e) qRT–PCR analysis of circIL4R and IL4R mRNA following RNase R treatment in CRC cells. (f) Actinomycin D chase assays were used to assess the stability of circIL4R and linear IL4R transcripts at various time points by qRT–PCR. (g, h) Subcellular distribution of circIL4R in CRC cells was determined by qRT–PCR of nuclear and cytoplasmic fractions and visualized using representative FISH images, showing predominant localization in the cytoplasm. $^{*}P < 0.05$, $^{**}P < 0.01$, $^{***}P < 0.001$.

Clinical significance of circIL4R in CRC patients

To explore the potential clinical relevance of circIL4R in colorectal cancer, we first examined its expression in a cohort of 120 CRC patients with follow-up information. Both qRT–PCR and FISH analyses revealed that circIL4R was significantly elevated in tumor tissues compared with adjacent normal tissues, corroborating the results obtained from the GEO database bioinformatic analysis **(Figures 2a–2d).** Considering the inherent stability of circRNAs, we assessed whether circIL4R could function as a diagnostic and prognostic marker for CRC.

Serum circIL4R levels were measured before and after surgery in a separate cohort of 50 CRC patients. A clear reduction in postoperative samples relative to preoperative levels was observed, suggesting that circIL4R reflects tumor burden **(Figure 2e).** Additionally, in an independent cohort of 40 healthy individuals and 40 CRC patients, serum circIL4R was significantly higher in patients than in controls **(Figure 2f).** To evaluate its diagnostic capability, we constructed a receiver operating characteristic (ROC) curve based on these data. The AUC for circIL4R was 0.718 (95% CI = 0.599–0.837), with a cutoff of 1.184 yielding a sensitivity of 60% and specificity of 87.5%, indicating its potential utility as a serum biomarker.

For comparison, the established marker CEA exhibited an AUC of 0.827 (95% CI = 0.736–0.917), exceeding that of circIL4R alone. Interestingly, combining circIL4R with CEA into a composite panel further improved diagnostic performance, achieving an AUC of 0.856 (95% CI = 0.773–0.938), highlighting the promise of this combined approach for CRC detection **(Figure 2g).**

Analysis of circIL4R expression in the larger cohort of 120 paired CRC tissues and ANTs revealed significant differences when patients were stratified by tumor pathological stage, T stage, N stage, and M stage, suggesting that circIL4R expression correlates with tumor progression and could provide prognostic information **(Figures 2h–2k).**

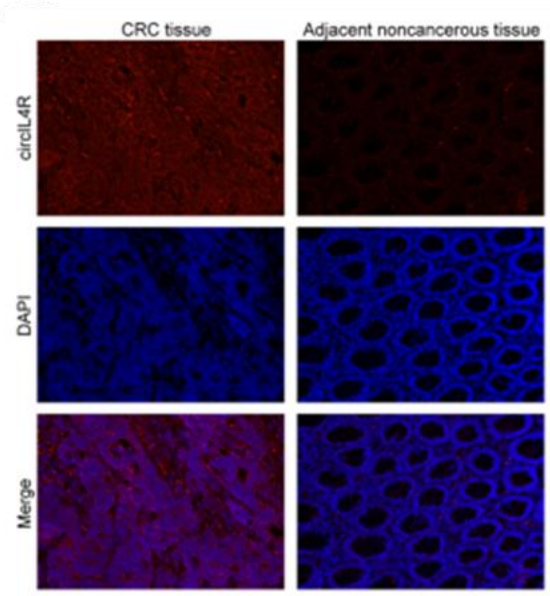

a)

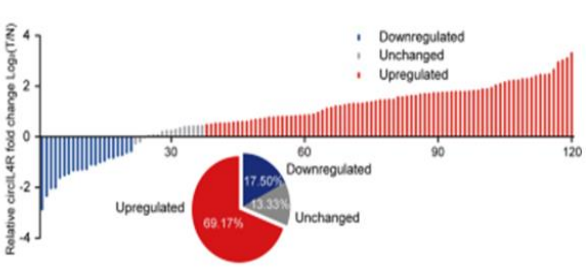

b)

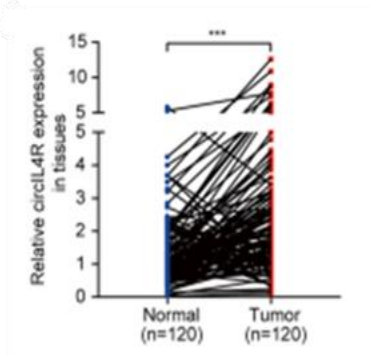
Relative circIL4R expression in tissues
***
Normal (n=120)
Tumor (n=120)

c)

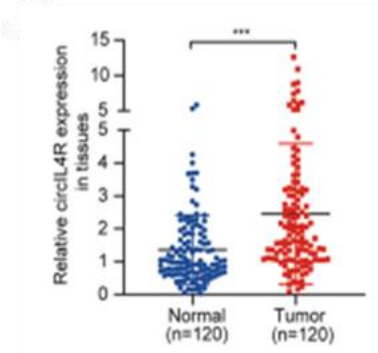
Relative circIL4R expression in tissues
***
Normal (n=120)
Tumor (n=120)

d)

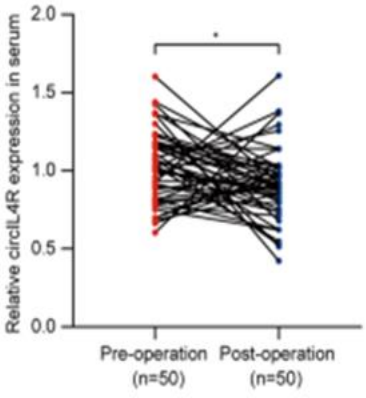
Relative circIL4R expression in serum
*
Pre-operation (n=50)
Post-operation (n=50)

e)

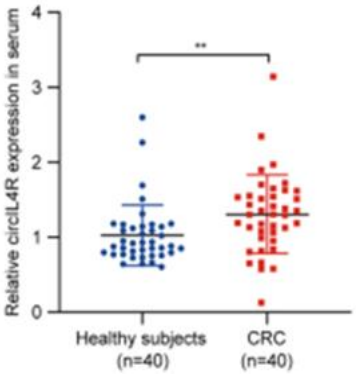
Relative circIL4R expression in serum
**
Healthy subjects (n=40)
CRC (n=40)

f)

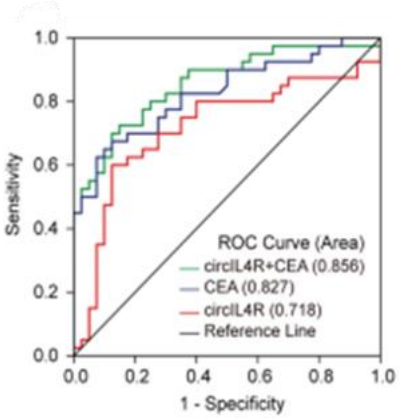
Sensitivity
1 - Specificity
ROC Curve (Area)
circIL4R+CEA (0.856)
CEA (0.827)
circIL4R (0.718)
Reference Line

g)

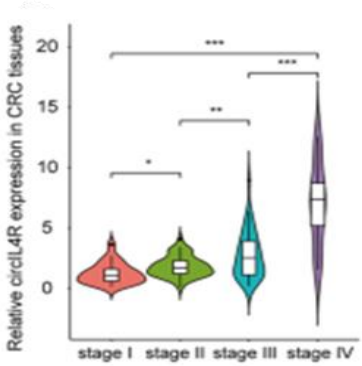
Relative circIL4R expression in CRC tissues
stage I
stage II
stage III
stage IV

h)

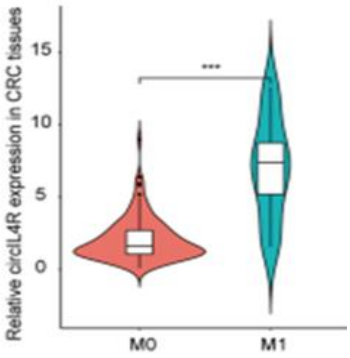
Relative circIL4R expression in CRC tissues
***
M0
M1

i)

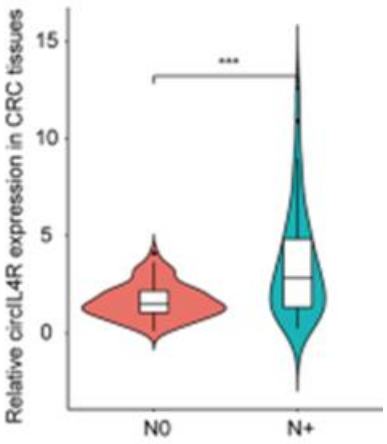

j)

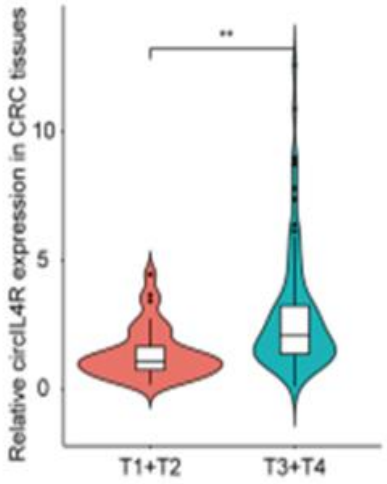

k)

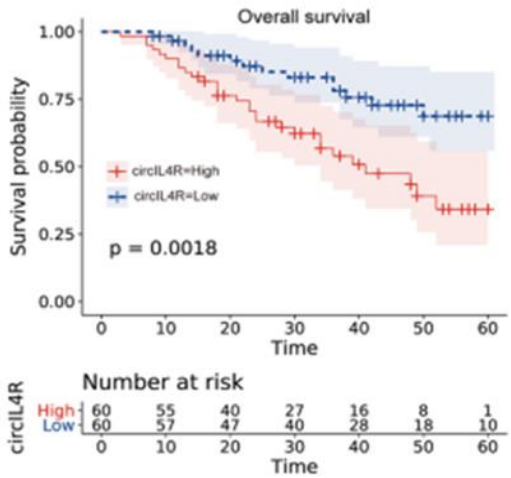

l)

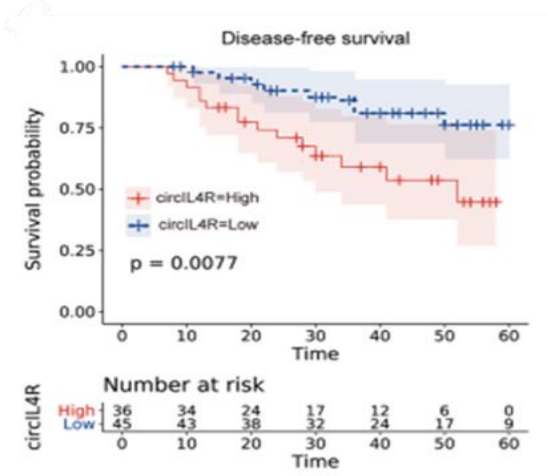

m)

Figure 2. Clinical importance of circIL4R in serum and CRC tissues. a Fluorescence in situ hybridization (FISH) demonstrated elevated circIL4R levels in CRC tissues relative to corresponding adjacent non-cancerous tissues (ANTs) (200× magnification). b-d qRT-PCR results indicated substantial upregulation of circIL4R in 120 CRC samples compared with matched ANTs. e Alterations in serum circIL4R concentrations were monitored by qRT-PCR in 50 CRC patients newly diagnosed, both prior to and following surgery. f qRT-PCR was used to quantify serum circIL4R in CRC patients (n = 40) and healthy subjects (n = 40). g The diagnostic utility of serum circIL4R, either independently or together with CEA, was evaluated using ROC curves. h-k circIL4R levels were displayed in violin plots for patient subgroups divided by clinical variables (pathological stage, M classification, N classification, T classification). l and m Patients with higher circIL4R in CRC showed diminished DFS (n = 120, P = 0.0077) and OS (n = 120, P = 0.0018) according to Kaplan–Meier curves derived from 120 specimens.

Chi-square tests were applied to explore links between circIL4R levels and clinicopathological variables. Elevated circIL4R correlated with unfavorable CRC traits, including greater tumor size (P = 0.022), increased invasion depth (P = 0.001), presence of lymph node metastasis (P = 0.010), distant metastasis (P = 0.038), and higher TNM stage (P = 0.003), implying that circIL4R contributes oncogenically to CRC metastasis and growth. However, no associations emerged with differentiation, gender, or age.

The prognostic role of circIL4R was assessed using follow-up data from 120 patients. Overexpression of circIL4R linked to inferior OS (P = 0.0018) and DFS (P = 0.0077) via Kaplan–Meier analysis **(Figures 2l and 2m)**. Univariate Cox models highlighted circIL4R, invasion depth, lymph node metastasis, differentiation, TNM stage, distant metastasis, and tumor diameter as key risk factors for OS or DFS .Multivariate models confirmed circIL4R as an independent predictor for DFS (HR, 2.927; 95% CI, 1.179–7.270; P = 0.021) and OS (HR, 2.077; 95% CI, 1.079–3.998; P = 0.029).

In situ hybridization (ISH) on TMAs with 179 paired ANT and CRC samples further showed much greater circIL4R in tumors than ANTs, particularly in stage III/IV versus I/II cases.Higher circIL4R also associated with larger tumors, deeper invasion, lymph node and distant metastasis, advanced TNM stage, and worse outcomes. In summary, circIL4R emerges as a promising prognostic indicator and possible treatment target for CRC.

TFAP2C drives circIL4R upregulation via transcriptional activation in CRC

To uncover the mechanism responsible for elevated circIL4R in CRC, we investigated the involvement of transcription factors (TFs), as previous studies indicate that TFs can influence circRNA levels by modulating transcription of host genes [26, 27]. Using the JASPAR database combined with BLAST analysis, we screened TFs predicted to bind the IL4R promoter region. TFAP2C emerged as a candidate due to the presence of two high-affinity binding motifs, termed TBS1 and TBS2, within the IL4R promoter **(Figure 3a).** TFAP2C has been reported to be upregulated in CRC and to act as an oncogene [28]. Analysis from the GEPIA database also revealed a positive correlation between TFAP2C and IL4R expression **(Figure 3b**).

To experimentally validate these findings, TFAP2C overexpression plasmids and specific siRNAs were transfected into CRC cells. Successful modulation of TFAP2C was confirmed by qRT–PCR and western blot **(Figures 3c and 3d).** We then assessed the impact of TFAP2C on IL4R expression by measuring pre-mRNA, mRNA, and circRNA levels using specific primers. Overexpression of TFAP2C markedly increased IL4R pre-mRNA, mRNA, and circIL4R, whereas TFAP2C knockdown led to a reduction in all three transcripts **(Figures 3e–3g).** These results suggest that TFAP2C enhances transcription of IL4R, which in turn promotes the production of both IL4R mRNA and circIL4R.

To further delineate the responsive regions, three fragments of the IL4R promoter were cloned into luciferase reporter constructs. Luciferase assays showed that the −1987/−913 fragment exhibited significant changes in activity depending on TFAP2C levels—reduced upon TFAP2C knockdown **(Figure 3h)** and increased with TFAP2C overexpression **(Figure 3i)**—whereas the −792/429 fragment remained unaffected **(Figures 3h and 3i).** These findings indicate that TFAP2C-binding elements reside within the −1987/−913 region.

Seven primer pairs (P1–P7) spanning the IL4R promoter were designed for ChIP-qPCR. TFAP2C binding was detected at P5–P7, with P5 and P6 corresponding to TBS1 and TBS2, respectively **(Figures 3j and k)**. Finally, analysis of TFAP2C mRNA in 120 CRC patient samples and protein detection by IHC in TMAs confirmed higher expression of TFAP2C in tumors compared with ANTs, which positively correlated with circIL4R levels **(Figures 3l–3n)**.

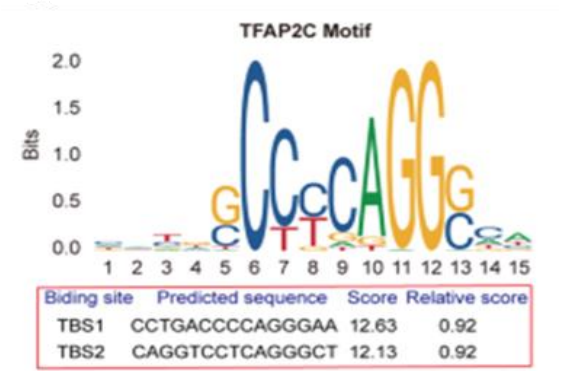

a)

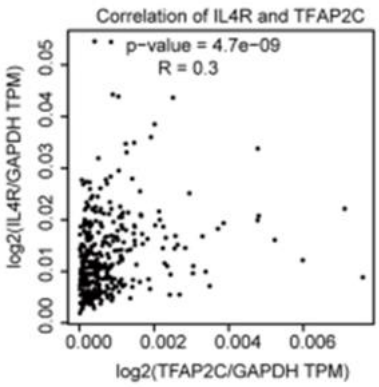

b)

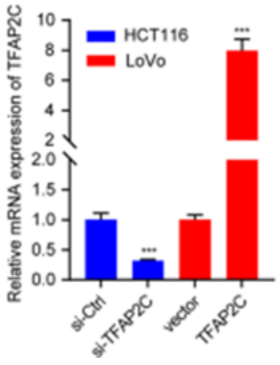
Relative mRNA expression of TFAP2C
HCT116
LoVo
si-Ctrl
si-TFAP2C
vector
TFAP2C

c)

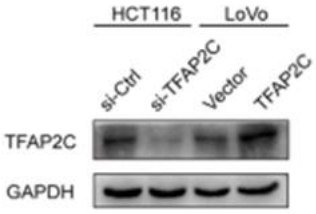
HCT116
LoVo
si-Ctrl
si-TFAP2C
Vector
TFAP2C
TFAP2C
GAPDH

d)

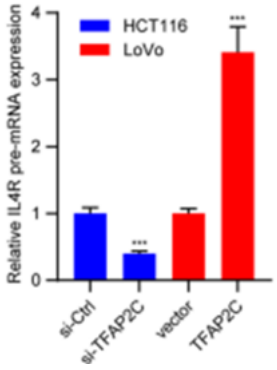
Relative IL4R pre-mRNA expression
HCT116
LoVo
si-Ctrl
si-TFAP2C
vector
TFAP2C

e)

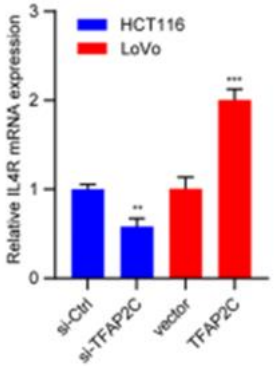
Relative IL4R mRNA expression
HCT116
LoVo
si-Ctrl
si-TFAP2C
vector
TFAP2C

f)

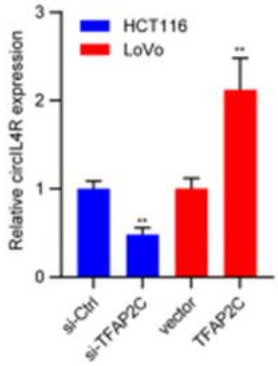
Relative circIL4R expression
HCT116
LoVo
si-Ctrl
si-TFAP2C
vector
TFAP2C

g)

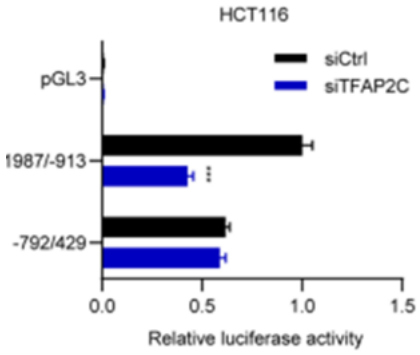
HCT116
siCtrl
siTFAP2C
pGL3
1987/-913
-792/429
Relative luciferase activity

h)

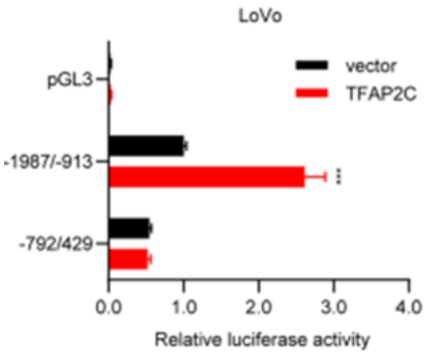
LoVo
vector
TFAP2C
pGL3
-1987/-913
-792/429
Relative luciferase activity

i)

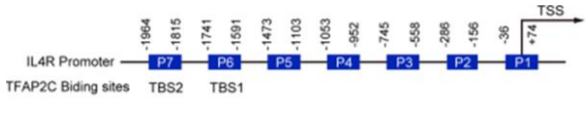
TSS
IL4R Promoter
TFAP2C Biding sites
TBS2
TBS1

j)

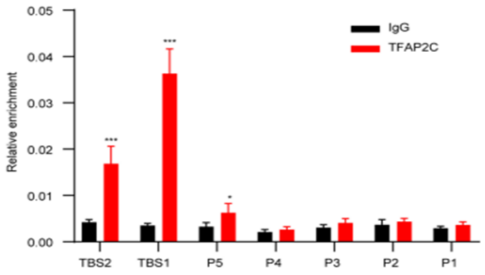
Relative enrichment
IgG
TFAP2C
TBS2
TBS1
P5
P4
P3
P2
P1

k)

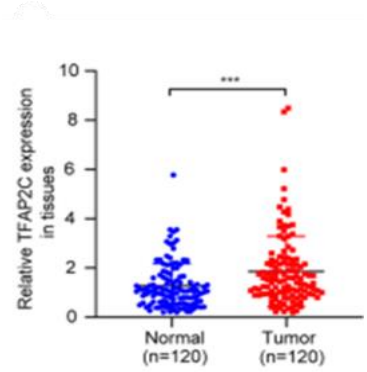

l)

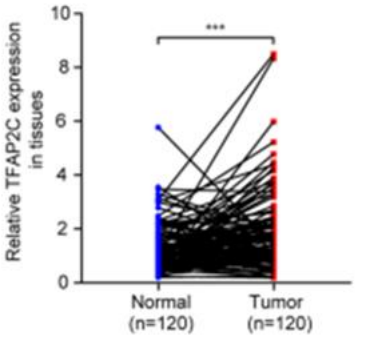

m)

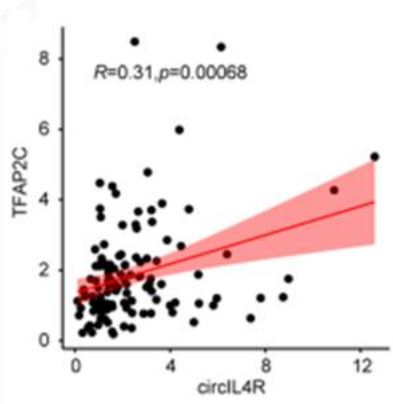

n)

Figure 3. TFAP2C upregulates circIL4R through transcriptional activation. (a) Using the JASPAR database, two potential TFAP2C-binding motifs in the IL4R promoter, named TBS1 and TBS2, were identified with high binding scores. (b) Analysis from the GEPIA dataset showed that TFAP2C expression positively correlates with IL4R in CRC. (c, d) qRT–PCR and western blot confirmed successful upregulation or knockdown of TFAP2C at both mRNA and protein levels in HCT116 and LoVo cells. (e–g) Overexpression of TFAP2C led to increased IL4R pre-mRNA, mRNA, and circIL4R levels, whereas TFAP2C silencing reduced all three transcripts. (h, i) Luciferase reporter assays demonstrated that the −1987/−913 fragment of the IL4R promoter is responsive to TFAP2C, with activity decreasing upon knockdown and increasing upon overexpression; the −792/429 fragment remained unresponsive. (j) Diagram of seven IL4R promoter regions (P1–P7) tested for TFAP2C binding (top) and illustration of predicted binding sites TBS1 and TBS2 (bottom). (k) ChIP-qPCR confirmed that TFAP2C binds P5–P7, including TBS1 and TBS2; IgG served as a negative control. (l, m) qRT–PCR analysis revealed significantly higher TFAP2C mRNA in 120 CRC tissues compared with paired ANTs. (n) TFAP2C levels positively correlated with circIL4R expression. $^{*}P < 0.05$, $^{**}P < 0.01$, $^{***}P < 0.001$.

CircIL4R drives proliferation, migration, and invasion of CRC cells in vitro

To determine the role of circIL4R in CRC cell behavior, we designed two siRNAs (si-circIL4R#1 and si-circIL4R#2) and a circIL4R overexpression plasmid. qRT–PCR confirmed that circIL4R was highly expressed in HCT116 and DLD1 cells and comparatively low in LoVo cells (**Figure 1b)**. Based on this, HCT116 and DLD1 cells were selected for knockdown experiments, and LoVo cells for overexpression studies. These manipulations did not alter IL4R mRNA levels (**Figures 4a and 4b)**

Stable knockdown cell lines (sh-circIL4R#1 and sh-circIL4R#2) were generated using lentiviral transduction. Functional assays including CCK-8, EdU incorporation, and colony formation revealed that depletion of circIL4R significantly inhibited CRC cell proliferation, while circIL4R overexpression enhanced growth **(Figures 4c–4h)**. These data suggest that circIL4R functions as a positive regulator of CRC cell proliferation.

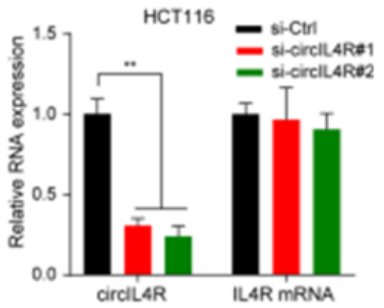

a)

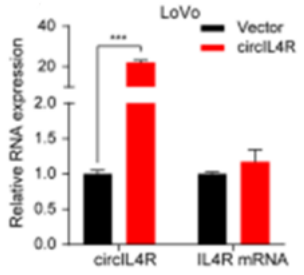
LoVo
Vector
circIL4R
Relative RNA expression
circIL4R
IL4R mRNA

b)

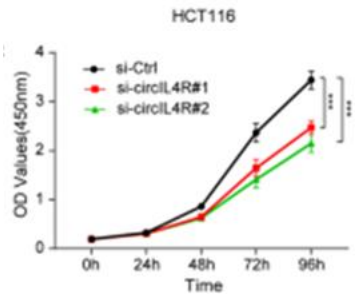
HCT116
si-Ctrl
si-circIL4R#1
si-circIL4R#2
OD Values(450nm)
Time
0h
24h
48h
72h
96h

c)

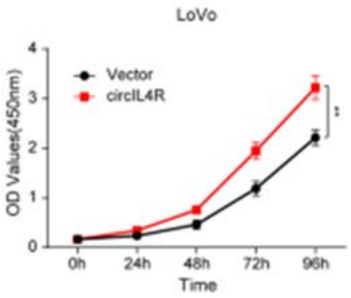
LoVo
Vector
circIL4R
OD Values(450nm)
Time
0h
24h
48h
72h
96h

d)

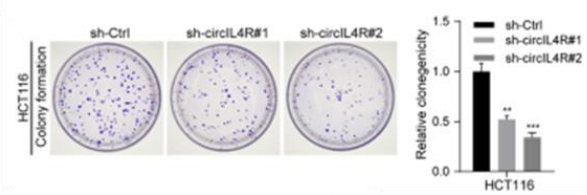
sh-Ctrl
sh-circIL4R#1
sh-circIL4R#2
HCT116
Colony formation
Relative clonegenicity

e)

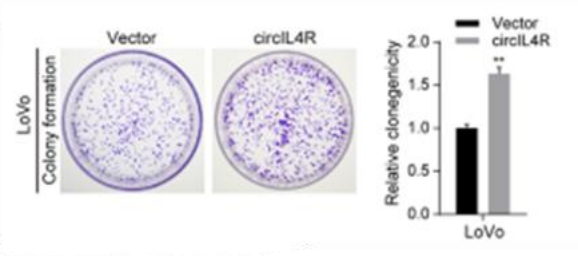
Vector
circIL4R
LoVo
Colony formation
Relative clonegenicity

f)

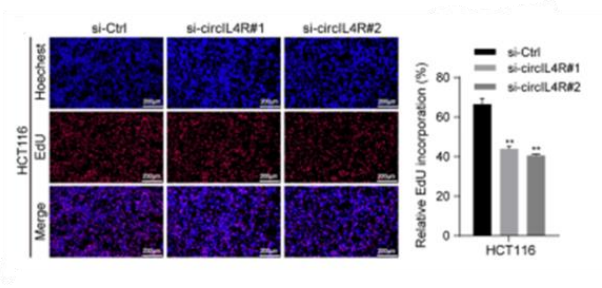
si-Ctrl
si-circIL4R#1
si-circIL4R#2
HCT116
Hoechst
EdU
Merge
Relative EdU incorporation (%)

g)

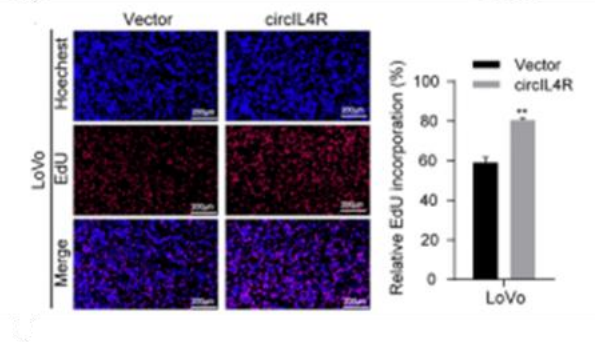
Vector
circIL4R
LoVo
Hoechst
EdU
Merge
Relative EdU incorporation (%)

h)

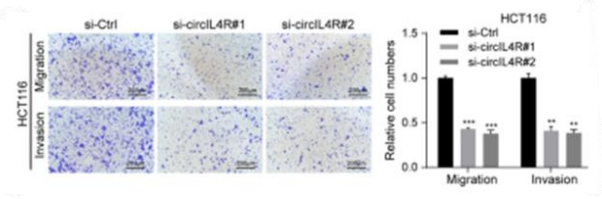
si-Ctrl
si-circIL4R#1
si-circIL4R#2
HCT116
Migration
Invasion
Relative cell numbers

i)

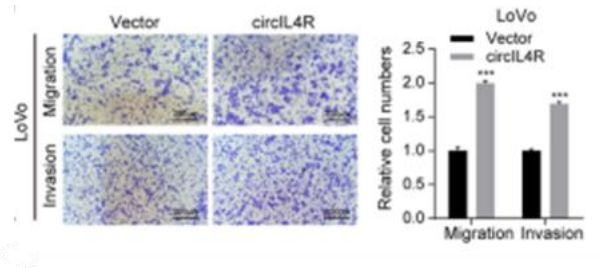
Vector
circIL4R
LoVo
Migration
Invasion
Relative cell numbers

j)

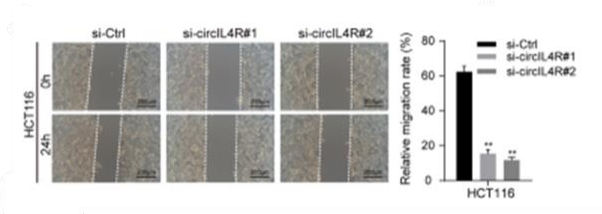
si-Ctrl
si-circIL4R#1
si-circIL4R#2
HCT116
0h
24h
Relative migration rate (%)

k)

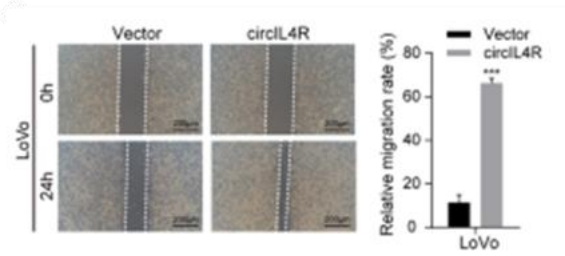

l)

Figure 4. circIL4R promotes proliferation, migration, and invasion of CRC cells in vitro. (a, b) qRT–PCR analysis of circIL4R and IL4R mRNA levels in HCT116 and LoVo cells following transfection with specific siRNAs or circIL4R overexpression plasmids. (c, d) CCK-8 assays showing the growth curves of CRC cells after circIL4R knockdown or overexpression at the indicated time points. (e, f) Colony formation assays evaluating the proliferative capacity of CRC cells stably expressing sh-circIL4R, sh-Ctrl, circIL4R, or vector control. (g, h) EdU incorporation assays assessing proliferation rates in transfected CRC cells. (i–l) Representative images and quantification of Transwell migration/invasion and wound healing assays in cells with circIL4R knockdown or overexpression. Data are shown as mean ± SD. $^{*}P < 0.05$, $^{**}P < 0.01$, $^{***}P < 0.001$.

Because higher circIL4R levels in patient tissues correlated with lymph node involvement, distant metastasis, and deeper tumor invasion, we next tested its role in CRC cell motility. Downregulation of circIL4R in HCT116 and DLD1 cells significantly reduced migration and invasion, while LoVo cells overexpressing circIL4R displayed enhanced motility and invasiveness **(Figures 4i–4l)**. Overall, these results indicate that circIL4R contributes to CRC cell growth and metastatic potential in vitro.

CircIL4R drives CRC progression through PI3K/AKT signaling

To explore the pathways mediating circIL4R's effects, we performed KEGG enrichment analysis of its predicted target genes, which highlighted the PI3K/AKT pathway **(Figure 5a),** a critical regulator of CRC cell proliferation and metastasis [29-31].

Western blot experiments confirmed that knocking down circIL4R in HCT116 and DLD1 cells decreased phosphorylated AKT and downstream effectors including Nanog, Cyclin D1 (CCND1), N-cadherin, Vimentin, and MMP2, while elevating p21 (CDKN1A) and E-cadherin levels. Total PI3K and AKT protein expression remained constant **(Figure 5b)**, suggesting that circIL4R specifically affects pathway activation rather than total protein abundance.

Rescue experiments using the PI3K/AKT activator 740Y-P and inhibitor LY294002 further validated this mechanism. In circIL4R knockdown cells, 740Y-P partially restored proliferation, migration, and invasion, whereas LY294002 counteracted the enhanced aggressive phenotype caused by circIL4R overexpression in LoVo cells **(Figures 5b–5j).**

These findings collectively demonstrate that circIL4R promotes CRC cell proliferation, migration, and invasion by activating the PI3K/AKT signaling cascade.

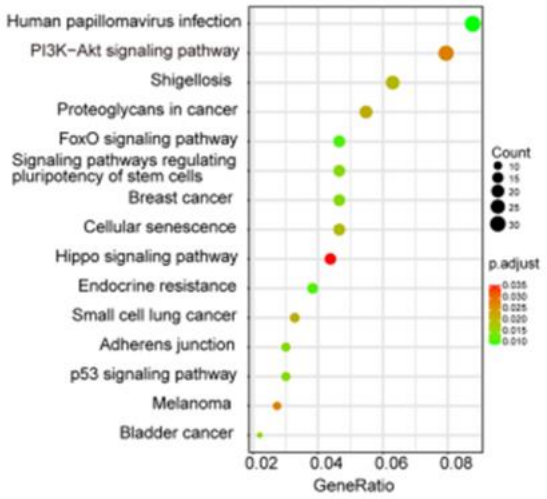

a)

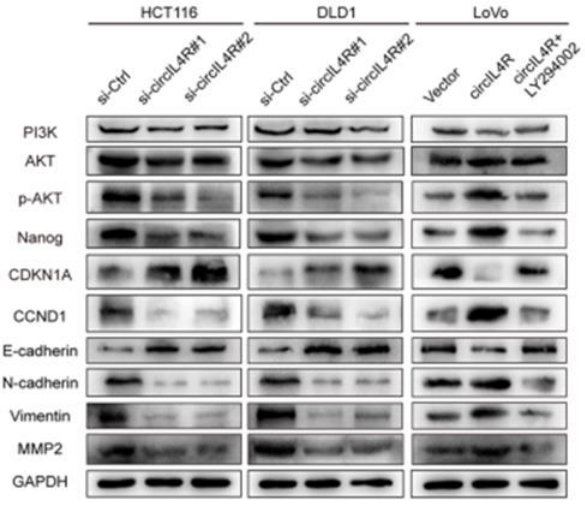

b)

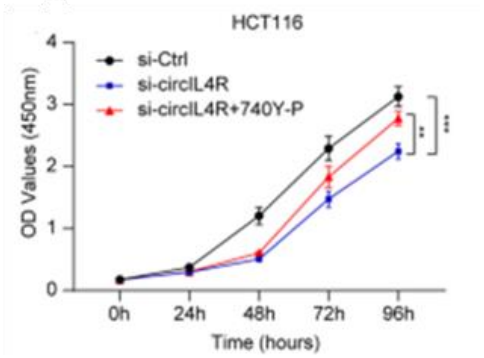
HCT116
si-Ctrl
si-circIL4R
si-circIL4R+740Y-P
OD Values (450nm)
Time (hours)
0h
24h
48h
72h
96h

c)

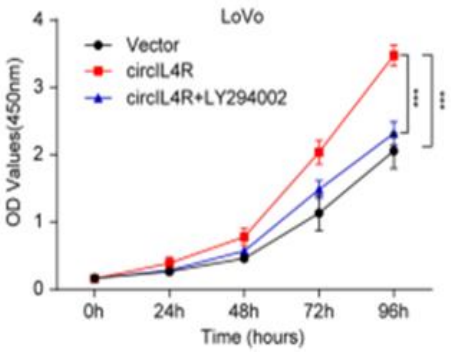
LoVo
Vector
circIL4R
circIL4R+LY294002
OD Values(450nm)
Time (hours)
0h
24h
48h
72h
96h

d)

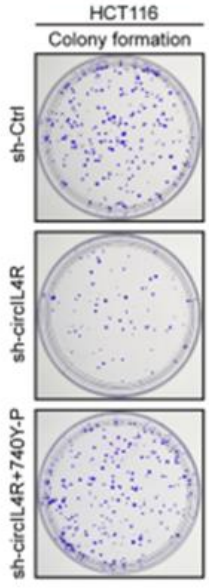
HCT116
Colony formation
sh-Ctrl
sh-circIL4R
sh-circIL4R+740Y-P

e)

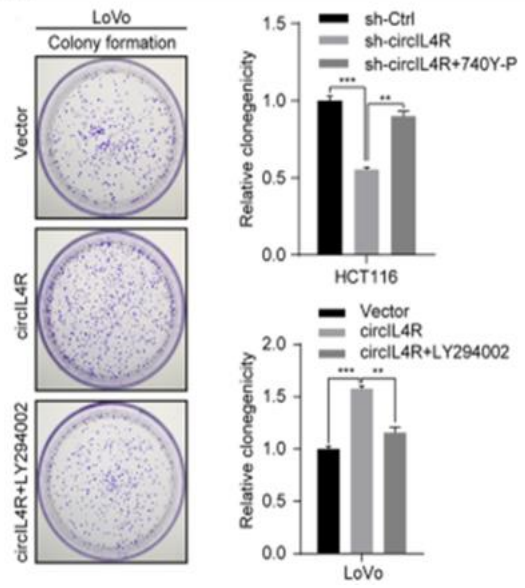
LoVo
Colony formation
Vector
circIL4R
circIL4R+LY294002
sh-Ctrl
sh-circIL4R
sh-circIL4R+740Y-P
Relative clonegenicity
HCT116
Vector
circIL4R
circIL4R+LY294002
Relative clonegenicity
LoVo

f)

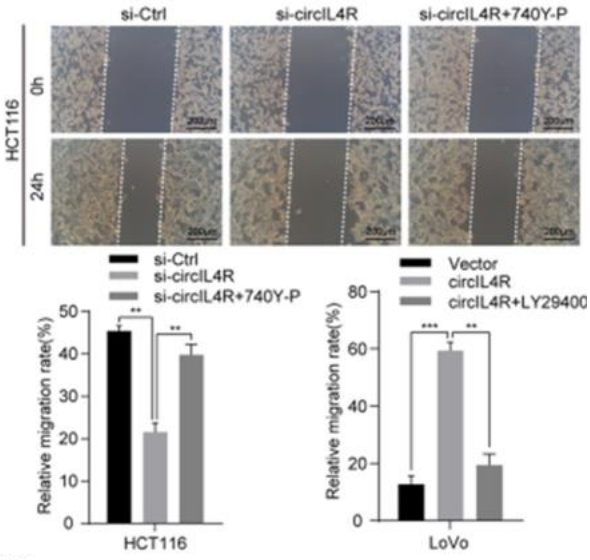
si-Ctrl
si-circIL4R
si-circIL4R+740Y-P
HCT116
0h
24h
si-Ctrl
si-circIL4R
si-circIL4R+740Y-P
Relative migration rate(%)
HCT116
Vector
circIL4R
circIL4R+LY29400
Relative migration rate(%)
LoVo

g)

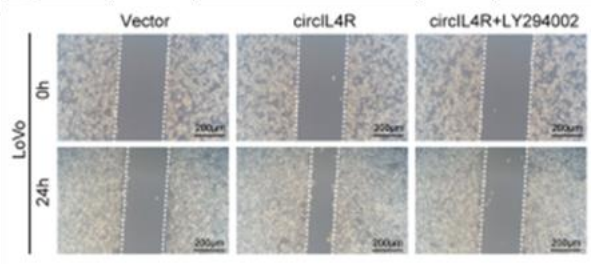
Vector
circIL4R
circIL4R+LY294002
LoVo
0h
24h

h)

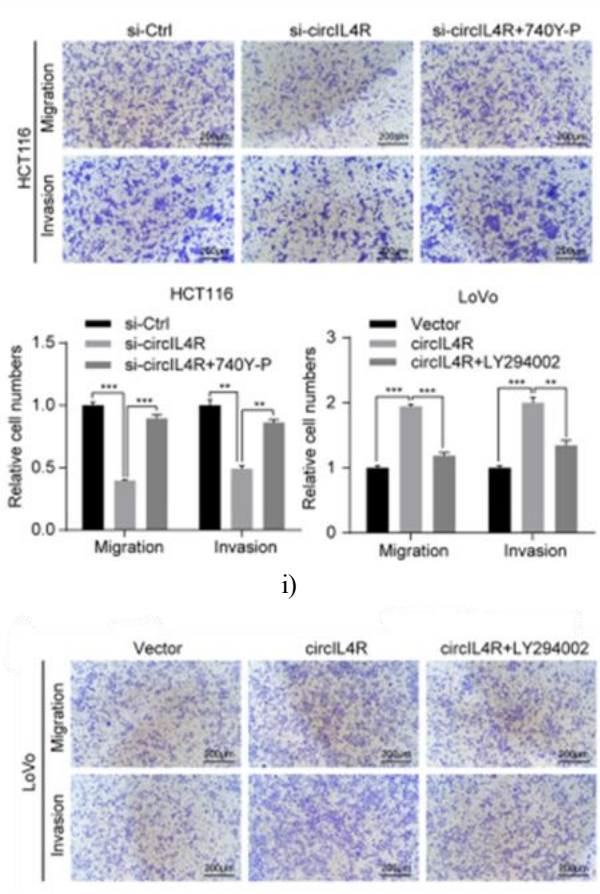

Figure 5. circIL4R regulates CRC progression through the AKT/ PI3K pathway. (a) KEGG enrichment analysis revealed that circIL4R is closely associated with the PI3K/AKT signaling pathway. (b) Western blot analysis showing expression changes of PI3K/AKT pathway proteins and downstream targets following circIL4R knockdown or overexpression in CRC cells, as well as the effects of the PI3K inhibitor LY294002. (c–f) Functional assays including CCK-8 and colony formation indicated that 740Y-P, a PI3K/AKT activator, partially rescued the decreased proliferation caused by circIL4R silencing in HCT116 cells. Conversely, LY294002 mitigated the proliferative effect of circIL4R overexpression in LoVo cells. (g–j) Transwell migration/invasion and wound healing assays demonstrated that the reduced motility and invasiveness of circIL4R-depleted HCT116 cells were reversed by 740Y-P, whereas LY294002 suppressed the enhanced invasion and migration caused by circIL4R overexpression in LoVo cells. Data are represented as mean ± SD. $^{*}P < 0.05$, $^{**}P < 0.01$, $^{***}P < 0.001$.

CircIL4R acts as a cytoplasmic sponge for miR-761 in CRC

Given its cytoplasmic localization, we hypothesized that circIL4R may modulate CRC progression by sequestering specific miRNAs [12]. Although previous reports suggested circIL4R sponges miR-541-3p in hepatocellular carcinoma [32], we found no significant effect of miR-541-3p in CRC cells.

To identify potential miRNA partners, we intersected predictions from Circular RNA Interactome, circBANK, and Starbase3.0, highlighting seven candidates (miR-513a-5p, miR-1286, miR-761, miR-3619-5p, miR-214-3p, miR-1184, miR-139-3p) detected in at least two databases **(Figure 6a).** Predicted binding sites of circIL4R are illustrated in **Figure 6b**.

RNA pull-down using a biotin-labeled circIL4R probe confirmed miR-761 as the most strongly enriched miRNA in HCT116 and DLD1 cells **(Figures 6c–6e).** To verify direct binding, we generated luciferase reporters containing either wild-type (WT) or mutated (Mut) circIL4R sequences corresponding to miR-761 binding sites **(Figure 6f).** Introduction of miR-761 mimics significantly reduced luciferase activity of the WT reporter, while the Mut reporter remained unaffected **(Figures 6g and 6h).**

Expression profiling in 120 CRC patient tissues revealed that miR-761 was markedly downregulated compared to adjacent normal tissues and inversely correlated with circIL4R **(Figures 6j–6l).** Similarly, miR-761 expression was lower in CRC cell lines than in FHC cells **(Figure 6i).** Double FISH assays confirmed cytoplasmic colocalization of circIL4R and miR-761 **(Figure 6m).**

Together, these data indicate that circIL4R functions as a miR-761 sponge, suggesting a post-transcriptional mechanism by which circIL4R promotes CRC cell proliferation, migration, and invasion.

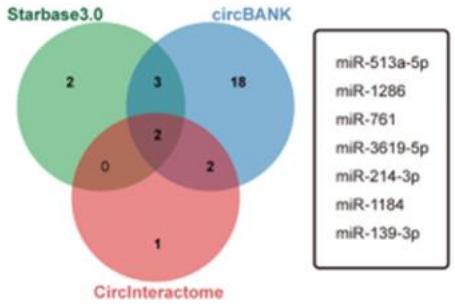

a)

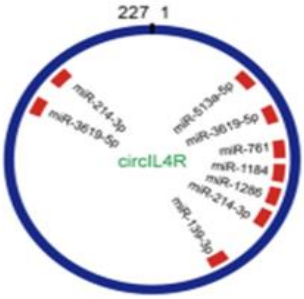
227 1
circIL4R
miR-214-3p
miR-3619-5p
miR-513a-5p
miR-3619-5p
miR-761
miR-1184
miR-1286
miR-214-3p
miR-139-3p

b)

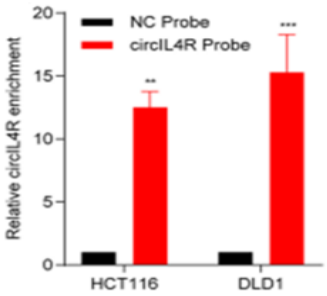
NC Probe
circIL4R Probe
Relative circIL4R enrichment
HCT116
DLD1

c)

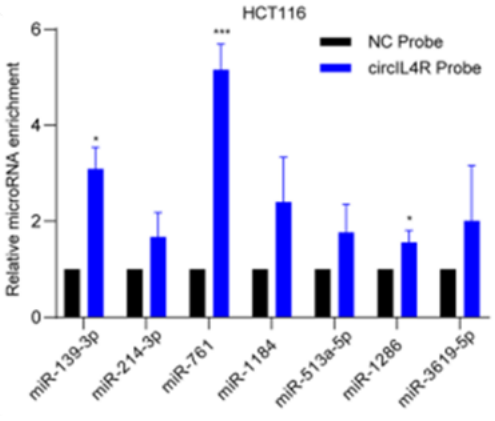
HCT116
NC Probe
circIL4R Probe
Relative microRNA enrichment
miR-139-3p
miR-214-3p
miR-761
miR-1184
miR-513a-5p
miR-1286
miR-3619-5p

d)

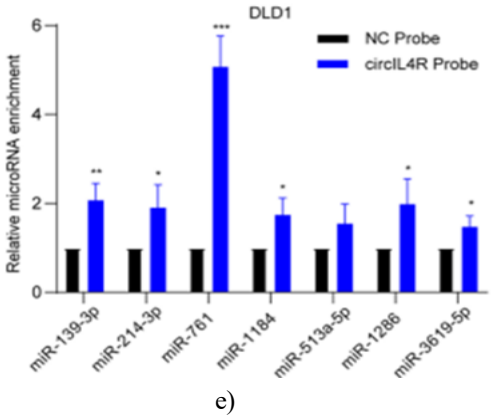
DLD1
NC Probe
circIL4R Probe
Relative microRNA enrichment
miR-139-3p
miR-214-3p
miR-761
miR-1184
miR-513a-5p
miR-1286
miR-3619-5p

e)

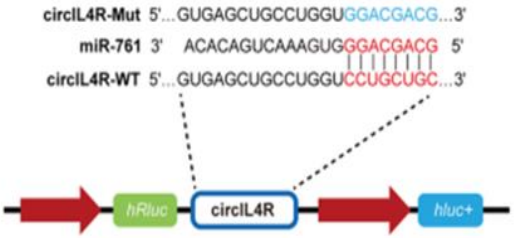
circIL4R-Mut 5'...GUGAGCUGCCUGGUGGACGACG...3'
miR-761 3' ACACAGUCAAAGUGGGACGACG 5'
circIL4R-WT 5'...GUGAGCUGCCUGGUCCUGCUGC...3'
hRluc
circIL4R
hluc+

f)

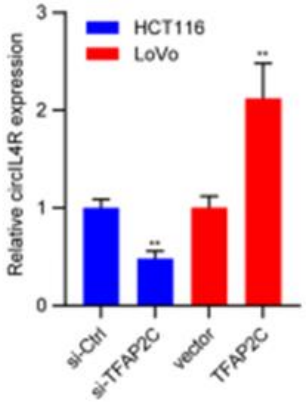
HCT116
LoVo
Relative circIL4R expression
si-Ctrl
si-TFAP2C
vector
TFAP2C

g)

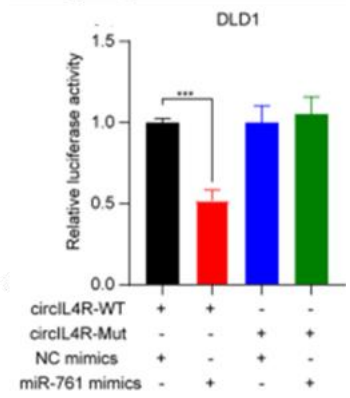
DLD1
Relative luciferase activity
circIL4R-WT
circIL4R-Mut
NC mimics
miR-761 mimics

h)

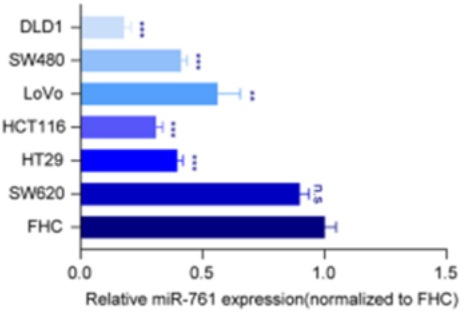
DLD1
SW480
LoVo
HCT116
HT29
SW620
FHC
Relative miR-761 expression(normalized to FHC)

i)

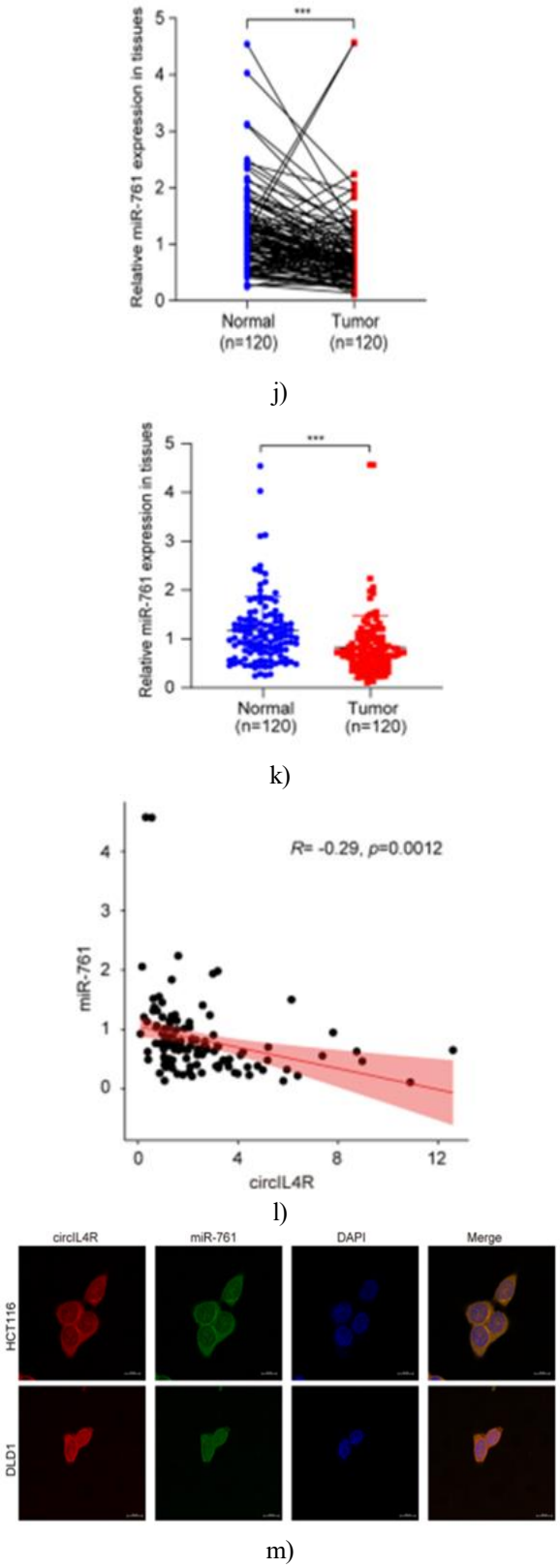

Figure 6. circIL4R functions as a cytoplasmic miR-761 sponge in CRC cells. (a) Seven candidate miRNAs predicted to bind circIL4R were identified by overlapping results from Circular RNA Interactome, circBANK, and Starbase3.0. (b) Diagram depicting the predicted binding sites of these miRNAs on circIL4R. (c) Verification of the biotin-labeled circIL4R probe's efficiency in CRC cells using qRT-PCR. (d, e) qRT-PCR analysis of the relative enrichment of candidate miRNAs captured by the circIL4R probe, highlighting miR-761 as the most enriched. (f) Design of wild-type (WT) and mutant (Mut) circIL4R luciferase reporters. (g, h) Luciferase assays showing that miR-761 mimics significantly reduced WT reporter activity but did not affect the Mut reporter. (i) Basal expression of miR-761 in FHC and CRC cell lines (DLD1, HT29, HCT116, SW620, LoVo, SW480). (j–l) qRT-PCR analysis of 120 CRC patient tissues showing decreased miR-761 expression relative to paired ANTs and a negative correlation with circIL4R levels. (m) FISH images confirmed co-localization of miR-761 and circIL4R in the cytoplasm; nuclei stained with DAPI. Scale bar: 10 μm. $^{*}P < 0.05$, $^{**}P < 0.01$, $^{***}P < 0.001$.

Previous studies have indicated that miR-761 suppresses CRC progression and inhibits PI3K/AKT signaling in other cancers [33, 34]. To determine whether circIL4R modulates PI3K/AKT signaling via miR-761, rescue experiments were conducted. CRC cells were co-transfected with either circIL4R overexpression or knockdown constructs alongside miR-761 mimics or inhibitors. qRT-PCR confirmed the efficiency of miR-761 modulation. Functional assays demonstrated that miR-761 overexpression reversed the enhanced migration, proliferation, and invasion driven by circIL4R in LoVo cells, while miR-761 inhibition rescued the suppressed malignant behaviors caused by circIL4R knockdown in HCT116 and DLD1 cells. Western blot analysis indicated that circIL4R knockdown-induced reductions in p-AKT levels were restored by miR-761 inhibition, whereas the activation of p-AKT by circIL4R overexpression was attenuated by miR-761 mimics. These findings indicate that circIL4R exerts oncogenic effects in CRC at least in part by sponging miR-761 and regulating PI3K/AKT signaling.

TRIM29 is a direct target of miR-761 in CRC

To explore downstream targets of miR-761, we conducted bioinformatic predictions using RNA22, Starbase3.0, miRTarBase and miRWalk. Integration of the four datasets identified 64 potential targets **(Figure**

7a). TRIM29 was prioritized due to its strong upregulation in CRC tissues and its presence among the top 25 overexpressed genes in TCGA **(Figures 7b and 7c)**. Analysis of GEO dataset GSE87211 confirmed elevated TRIM29 expression in CRC samples **(Figure 7d).**

Functional validation showed that transfection of miR-761 mimics decreased TRIM29 mRNA and protein levels, while miR-761 inhibition led to increased TRIM29 expression in CRC cells **(Figures 7e and 7f).** To confirm direct targeting, luciferase reporters containing WT or Mut TRIM29 3′-UTR sequences were constructed **(Figure 7g).** miR-761 mimics suppressed WT reporter activity but had no effect on the Mut reporter, indicating direct interaction between miR-761 and the TRIM29 3′-UTR **(Figures 7h and 7i).**

Clinically, TRIM29 expression was significantly elevated in 120 CRC patient tissues, showing an inverse correlation with miR-761 and a positive correlation with circIL4R **(Figures 7j–7m).** IHC analysis of TMAs confirmed higher TRIM29 protein levels in CRC compared to ANTs and a positive association with circIL4R. These results collectively demonstrate that TRIM29 is a direct downstream effector of miR-761 in CRC.

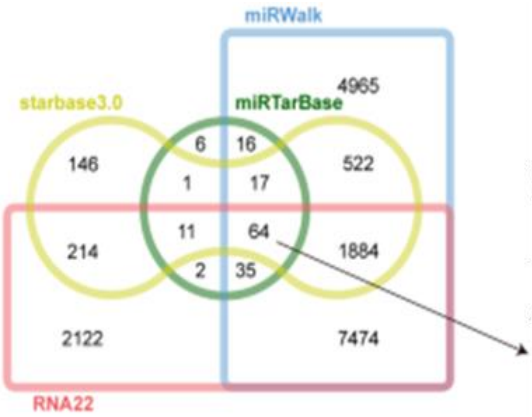

a)

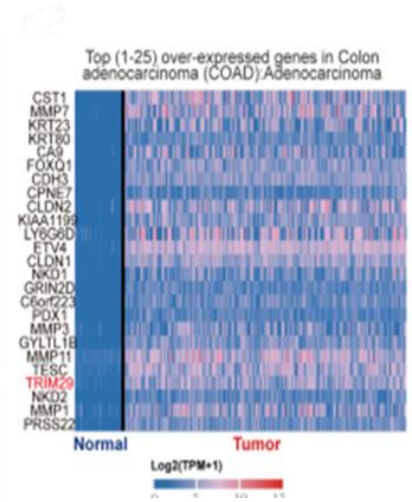

b)

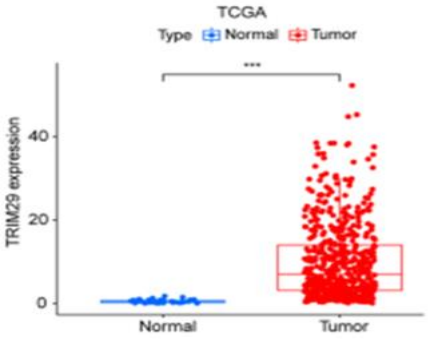

c)

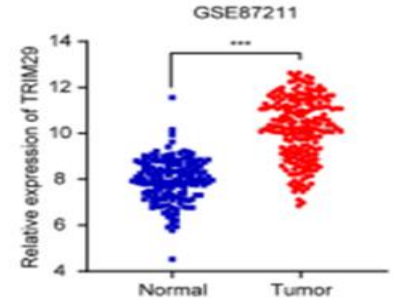

d)

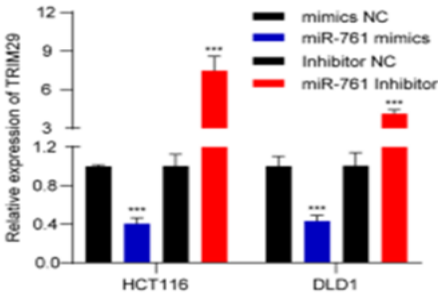

e)

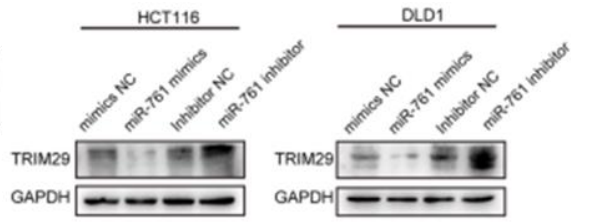

f)

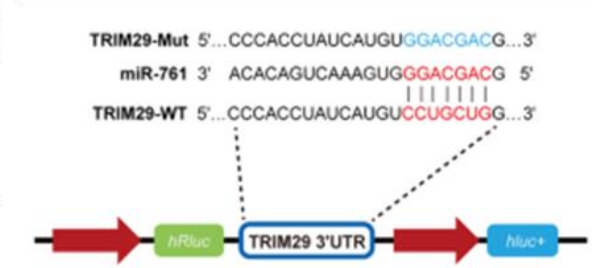

g)

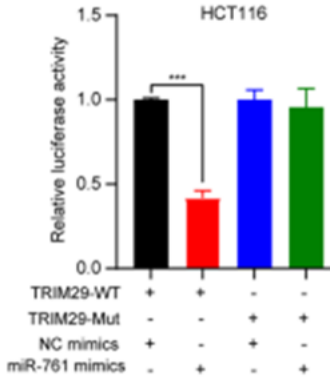

h)

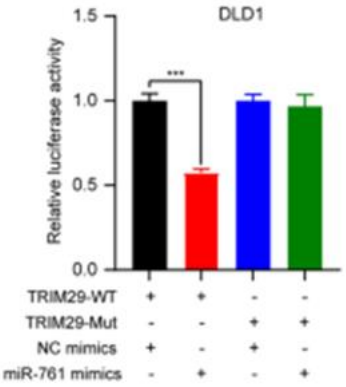

i)

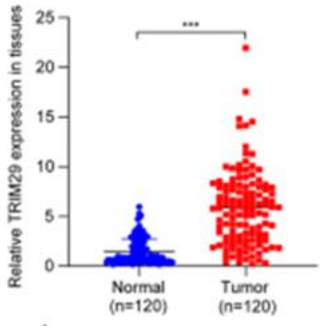

j)

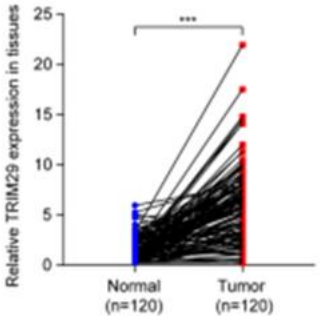

k)

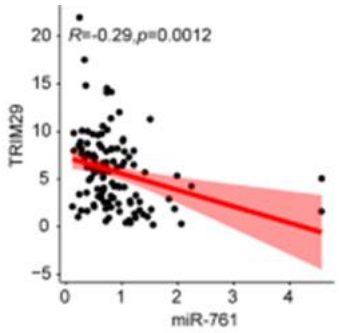

l)

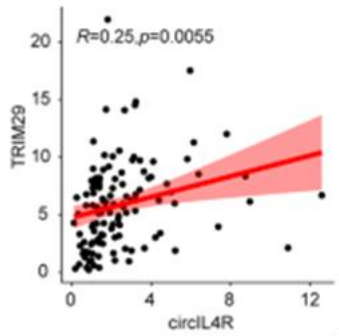

m)

Figure 7. TRIM29 functions as a downstream target of miR-761. (a) Venn diagram illustrating the overlapping genes predicted as targets of miR-761 using RNA22, starbase3.0, miRTarBase and miRWalk databases. (b) Heatmap displaying the 25 most upregulated genes in the TCGA-COAD dataset. (c) Comparison of TRIM29

mRNA expression between CRC tumors and matched normal tissues in TCGA. (d) TRIM29 expression levels in primary colorectal tumors versus normal tissues from the GEO dataset. (e, f) Assessment of TRIM29 mRNA and protein levels in CRC cells transfected with miR-761 mimics or inhibitors via qRT-PCR and western blotting. (g) Schematic representation of luciferase reporter constructs containing mutant (Mut) or wild-type (WT) TRIM29 3′-UTR sequences. (h, i) Luciferase assays showing that miR-761 mimics reduce activity of the TRIM29 WT reporter but do not affect the Mut reporter in CRC cells. (j, k) qRT-PCR results showing that TRIM29 expression is significantly higher in 120 CRC patient tissues compared with paired adjacent normal tissues (ANTs). (l, m) Correlation analysis indicating TRIM29 positively correlates with circIL4R and inversely correlates with miR-761. $^{*}P < 0.05$, $^{**}P < 0.01$, $^{***}P < 0.001$.

CircIL4R promotes CRC progression through the PI3K/AKT signaling and miR-761/TRIM29 axis

To investigate the interplay between circIL4R and TRIM29, CRC cells were either transfected with a TRIM29-targeting siRNA (si-TRIM29) to inhibit its expression or with a TRIM29 overexpression plasmid [22, 23]. Efficient modulation of TRIM29 was confirmed by qRT-PCR and western blotting.

Functional assays, including CCK-8, colony formation, Transwell migration, and wound healing assays, demonstrated that TRIM29 overexpression stimulated CRC cell proliferation, invasion and migration, whereas TRIM29 knockdown suppressed these behaviors **(Figures 8a–8d).** Importantly, the diminished proliferative and migratory capacities caused by circIL4R silencing in HCT116 cells were rescued upon TRIM29 overexpression, while the tumor-promoting effects of circIL4R overexpression in LoVo cells were largely reversed by TRIM29 knockdown **(Figures 8a–8d).**

Western blot analysis further revealed that circIL4R regulates PI3K/AKT pathway activation via TRIM29. Specifically, the reduction of phosphorylated AKT (p-AKT) following circIL4R knockdown in HCT116 cells was restored by TRIM29 overexpression, whereas the elevated p-AKT levels caused by circIL4R overexpression in LoVo cells were blocked upon TRIM29 silencing **(Figure 8e).**

Overall, these results indicate that circIL4R drives CRC cell proliferation, migration, and invasion primarily through the miR-761/TRIM29 axis by modulating PI3K/AKT signaling, suggesting that circIL4R represents a promising target for therapeutic intervention.

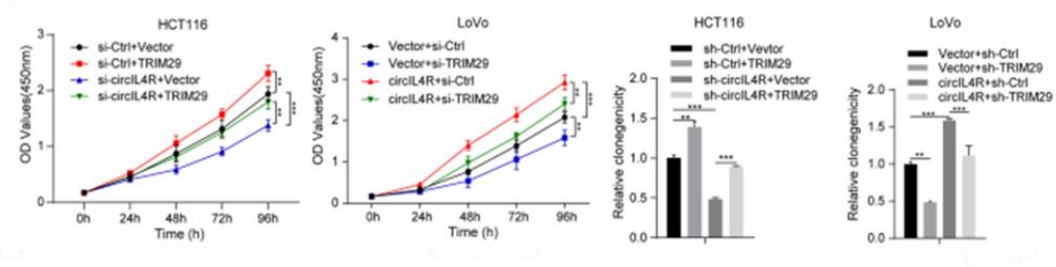

a)

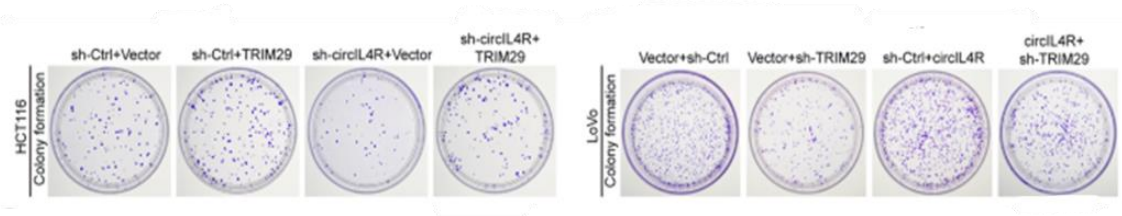

b)

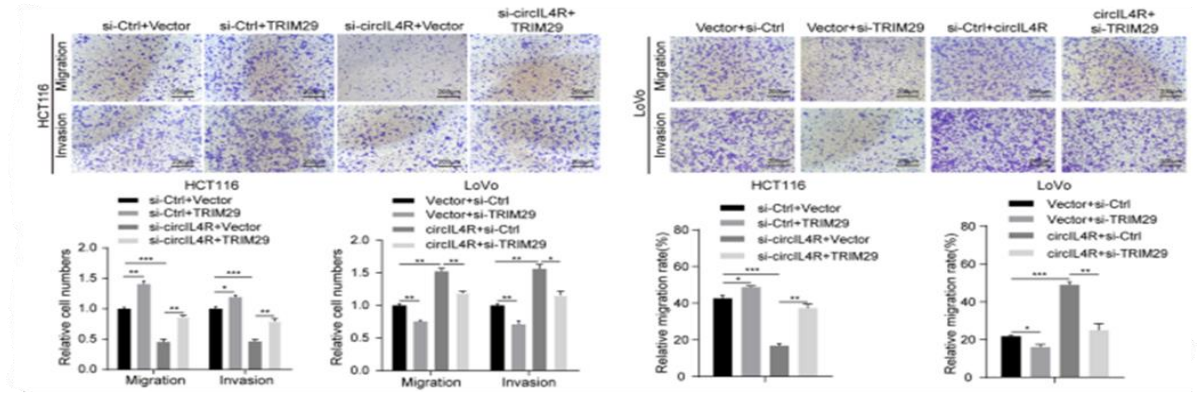

c)

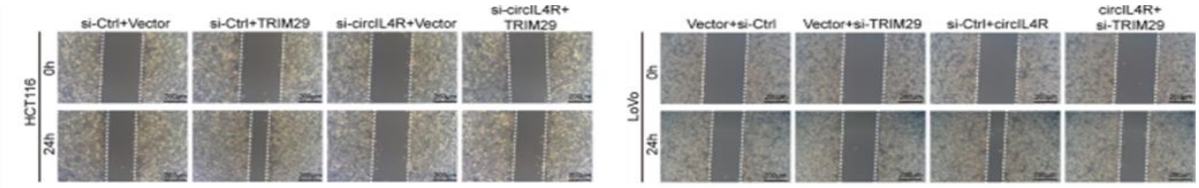

d)

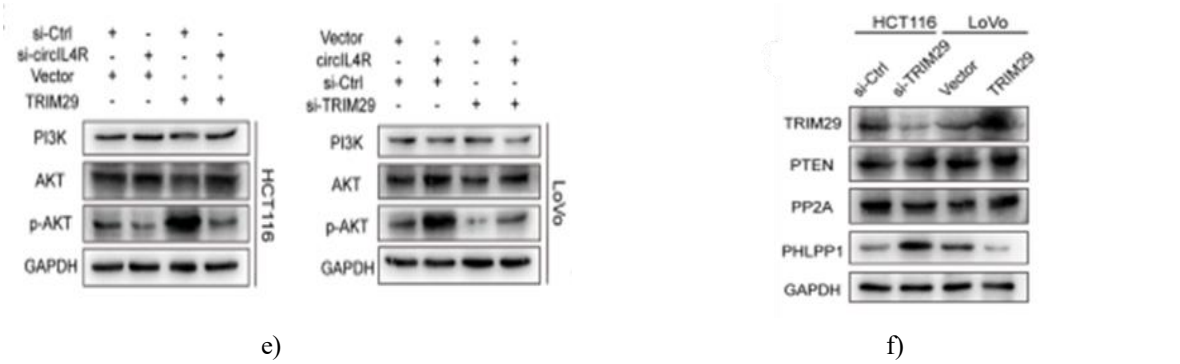

e) f)

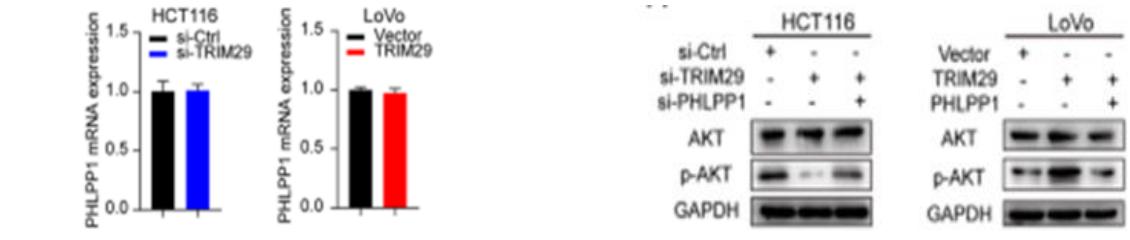

g) h)

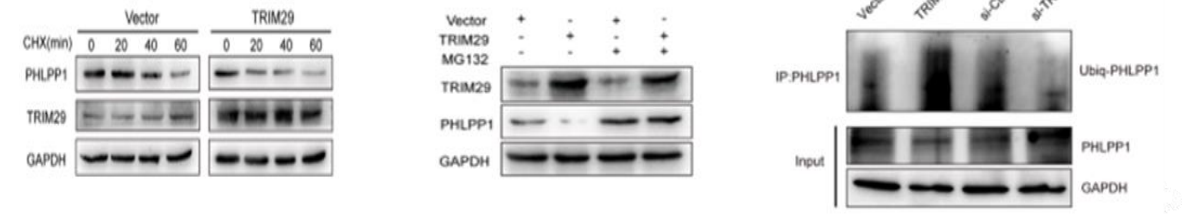

i) j) k)

Figure 8. CircIL4R Drives Colorectal Cancer Progression via the circIL4R/miR-761/TRIM29/PHLPP1 Pathway. a and b Using CCK-8 and colony formation experiments, we found that TRIM29 overexpression counteracted the proliferation suppression induced by circIL4R silencing in HCT116 cells. In LoVo cells, TRIM29 silencing

eliminated the proliferation enhancement caused by circIL4R overexpression. c and d Quantitative data and representative images from wound healing and Transwell assays indicated that overexpression of TRIM29 restored migration and invasion abilities suppressed by circIL4R knockdown in HCT116 cells. Knockdown of TRIM29, in turn, blocked the increased migration and invasion promoted by circIL4R overexpression in LoVo cells. e In Western blot results, TRIM29 overexpression restored the lowered p-AKT levels in HCT116 cells after circIL4R knockdown. Conversely, TRIM29 knockdown reduced the elevated p-AKT levels in LoVo cells following circIL4R overexpression. f Protein expression levels of PTEN, PP2A, and PHLPP1 were assessed by Western blotting in CRC cells after transfection with TRIM29 overexpression plasmids or siRNAs. g qRT-PCR was employed to measure PHLPP1 mRNA expression in CRC cells transfected with TRIM29 siRNAs or overexpression plasmids. h Western blotting evaluated p-AKT levels in HCT116 cells with siTRIM29 transfection alone or combined with siPHLPP1 (left), and in LoVo cells with TRIM29 overexpression alone or together with PHLPP1 overexpression (right). i The protein-protein interaction between TRIM29 and PHLPP1 in HCT116 cells was confirmed using co-immunoprecipitation and subsequent Western blot analysis. j To assess PHLPP1 protein stability under TRIM29 overexpression in HCT116 cells, Western blots were performed after cycloheximide (CHX, 100 μg/ml) treatment to inhibit protein synthesis, with samples collected at indicated time points. k Following treatment with the proteasome inhibitor MG132 (10 μM) in HCT116 cells, Western blot analysis of ubiquitinated proteins revealed that TRIM29 overexpression led to proteasome-dependent degradation of PHLPP1. l The influence of TRIM29 knockdown or overexpression on PHLPP1 ubiquitination in HCT116 cells was examined through Western blot assays. $^{*}P < 0.05$, $^{**}P < 0.01$, $^{***}P < 0.001$.

circIL4R facilitates PI3K/AKT activation via TRIM29-dependent PHLPP1 degradation

circIL4R promotes TRIM29 expression by acting as a sponge for miR-761, and overexpressing TRIM29 alone is sufficient to activate the PI3K/AKT pathway. This led us to investigate how circIL4R regulates PI3K/AKT through the miR-761/TRIM29 axis. Earlier studies reported that TRIM29 overexpression in nasopharyngeal carcinoma suppresses PTEN, leading to PI3K/AKT pathway activation [35]. Tumor suppressors such as PTEN, PP2A, and PHLPP1 are known to negatively regulate this signaling cascade [36–38]. To determine whether TRIM29 acts similarly in CRC, we performed western blotting. The results showed that manipulating TRIM29 levels did not affect PTEN or PP2A, but knockdown of TRIM29 increased PHLPP1 protein, while TRIM29 overexpression reduced it, without altering PHLPP1 mRNA **(Figures 8f and 8g).** Additionally, TRIM29 depletion lowered p-AKT levels, and this effect was reversed when PHLPP1 was simultaneously silenced **(Figure 8h).** These observations suggest that TRIM29 modulates PI3K/AKT activity in CRC by post-transcriptionally regulating PHLPP1.

PHLPP1 is known to be regulated via post-translational modifications, including ubiquitination [39]. TRIM29, an E3 ubiquitin ligase, promotes tumor progression by targeting proteins such as STING and ISG15 for degradation [19, 40]. Interestingly, TRIM11, a TRIM family member, has been shown to trigger PHLPP1 ubiquitination and activate PI3K/AKT [41], hinting at a similar role for TRIM29. Co-immunoprecipitation confirmed that endogenous TRIM29 interacts with PHLPP1 in HCT116 cells **(Figure 8i)**. Cycloheximide chase assays demonstrated that PHLPP1 protein stability was reduced in cells overexpressing TRIM29 **(Figure 8j),** and this degradation was blocked by the proteasome inhibitor MG132 **(Figure 8k),** supporting ubiquitin-dependent regulation. Ubiquitination assays further revealed that PHLPP1 ubiquitination decreased with TRIM29 knockdown and increased with its overexpression **(Figure 8l).** Collectively, these data indicate that circIL4R enhances PI3K/AKT signaling through TRIM29-mediated ubiquitination and degradation of PHLPP1.

circIL4R drives CRC growth and metastasis in vivo

To explore circIL4R's role in tumor growth, HCT116 and DLD1 cells with stable circIL4R knockdown (sh-circIL4R) or control (sh-Ctrl) were implanted subcutaneously in BALB/c nude mice **(Figure 9a).** Tumors from the circIL4R-depleted cells grew significantly slower, with smaller volume and lower weight than controls **(Figures 9b–9e).** Immunohistochemistry showed reduced Ki-67, TRIM29, and p-AKT staining, alongside elevated PHLPP1 in sh-circIL4R tumors **(Figure 9f).**

For metastasis assessment, luciferase-labeled CRC cells were injected via the tail vein. circIL4R knockdown

markedly decreased lung metastases, as evidenced by lower fluorescence and fewer nodules **(Figures 9g–9j)**. Correspondingly, mice bearing sh-circIL4R tumors exhibited improved survival **(Figures 9k and 9l).** These in vivo results align with in vitro data, confirming that circIL4R promotes CRC proliferation and metastasis.

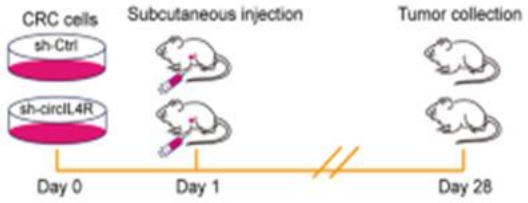

a)

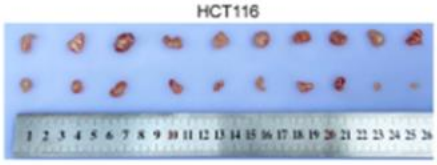

b)

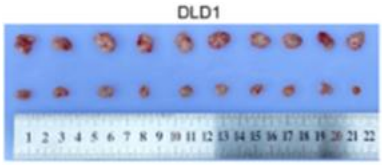

c)

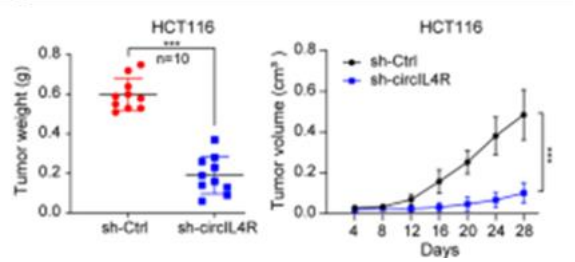

d)

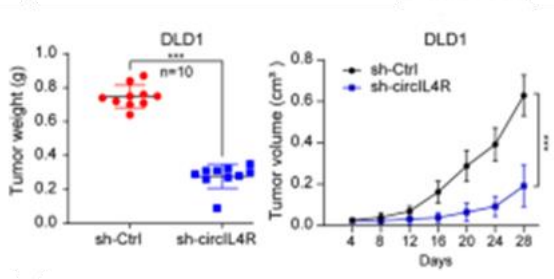

e)

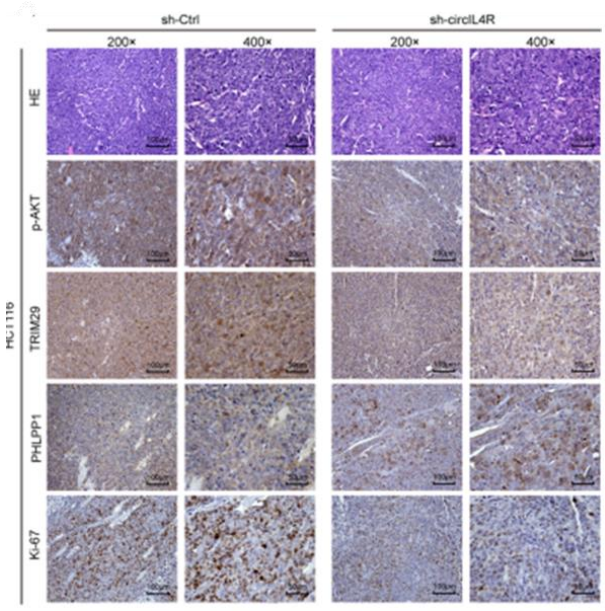

f)

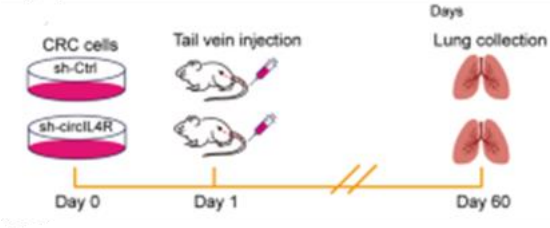

g)

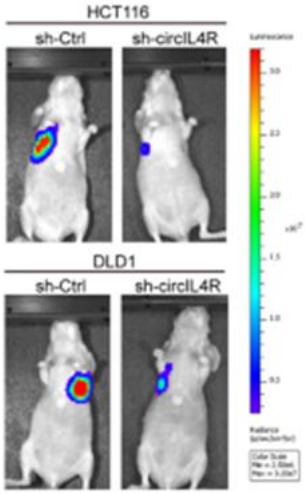

h)

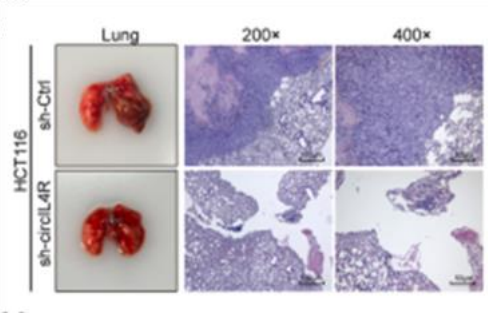

i)

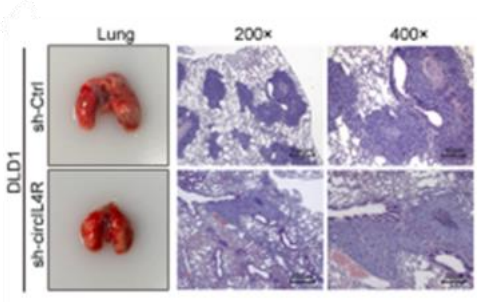

j)

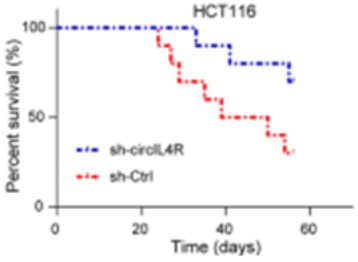

k)

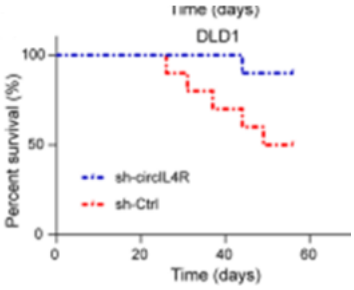

l)

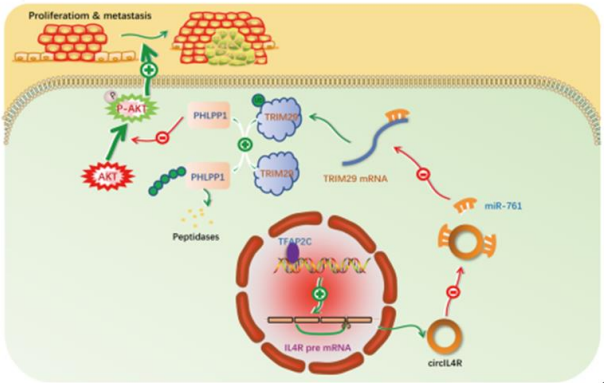

m)

Figure 9. circIL4R enhances CRC tumor growth and metastasis in vivo. (a) Diagram depicting the subcutaneous xenograft model using BALB/c nude mice. (b, c) Representative images of dissected xenograft tumors from mice injected with control or circIL4R-silenced CRC cells. (d, e) Tumor growth curves and weight measurements show that circIL4R knockdown significantly reduces tumor growth and mass. (f) H&E and IHC staining of xenograft tumor sections revealed that circIL4R depletion decreased Ki-67, TRIM29, and p-AKT levels while increasing PHLPP1 expression. (g) Schematic of the tail vein injection model used to evaluate CRC metastasis in vivo. (h) Representative images and quantification of luminescence intensity demonstrated reduced lung metastases in circIL4R knockdown mice (n = 5 per group). (i, j) HE-stained images of lungs confirm fewer metastatic nodules in the circIL4R-depleted group. (k, l) Kaplan–Meier survival curves indicate that mice with circIL4R-silenced CRC cells have prolonged overall survival compared with control mice. (m) Proposed model illustrating how circIL4R promotes CRC proliferation and metastasis through the miR-761/TRIM29/PHLPP1 axis, leading to activation of the PI3K/AKT signaling pathway. $^{*}P < 0.05$, $^{**}P < 0.01$, $^{***}P < 0.001$.

Despite significant advances in the clinical management of CRC over the past decades, patient prognosis remains unsatisfactory. This underscores the urgent need to identify reliable therapeutic targets and understand their roles in CRC progression. In recent years, circRNAs have attracted increasing attention due to their unique biogenesis, expression patterns, functional roles, and clinical relevance across various cancers [42]. With the widespread adoption of high-throughput sequencing and

circRNA-specific bioinformatics tools, comprehensive circRNA datasets are now publicly accessible, providing opportunities for both bioinformatic analysis and clinical validation.

In this study, we identified a novel circRNA, circIL4R, which was consistently upregulated in CRC tissues, cell lines, and microarray analyses. Its expression was closely associated with aggressive clinicopathological features and poor prognosis in CRC patients. Considering the advantages of noninvasive biomarkers—including cost-effectiveness, repeatability, and clinical utility for patient management [43]—circRNAs, owing to their high abundance, tissue-specific expression, and covalently closed structure, are promising candidates for liquid biopsy applications [44]. Our results revealed that serum circIL4R levels were significantly altered in CRC patients before and after surgery and differed from healthy controls. Moreover, serum circIL4R showed high sensitivity and specificity for CRC diagnosis and postoperative monitoring, highlighting its potential as a liquid biopsy biomarker.

However, several challenges remain before circRNAs can be applied clinically. For example, the presence of a back-spliced junction (BSJ) restricts the design of specific primers and probes, necessitating more sensitive and precise detection methods [6]. Additionally, most studies on circRNA biomarkers have involved small patient cohorts, and larger prospective studies are needed to validate their diagnostic and prognostic utility [45]. Optimizing detection methods, establishing clinical cutoff values, and combining circRNAs with traditional biomarkers, such as CEA, may further improve clinical applicability. Overall, despite these obstacles, circIL4R shows promise for large-scale CRC screening and real-time monitoring of disease progression and treatment response.

Previous studies have demonstrated that circRNAs are often upregulated in cancers and correlate with tumorigenesis. Yet, the upstream mechanisms driving circRNA overexpression remain poorly understood. For instance, Meng *et al*. reported that Twist can induce circ10720 expression by binding its host gene promoter [27]. In line with these findings, our data revealed that TFAP2C promotes circIL4R overexpression via transcriptional activation of its host gene. This observation is consistent with reports that TFAP2C can regulate lncRNA expression through transcriptional activation [46, 47]. Additionally, RNA-binding proteins (RBPs), such as EIF4A3 and FUS, have been shown to enhance circRNA biogenesis by interacting with flanking intronic sequences [48, 49]. Whether RBPs also contribute to circIL4R formation, splicing, transport, or degradation warrants further investigation.

Our clinical analyses indicated that high circIL4R expression correlates with increased tumor size, lymph node involvement, and distant metastasis, suggesting its role in promoting CRC proliferation and dissemination. Functional experiments in vitro demonstrated that circIL4R enhances CRC cell proliferation, migration, and invasion. Consistently, in vivo studies showed that circIL4R knockdown reduced tumor growth in a subcutaneous xenograft model and decreased metastatic colonization in a tail vein injection model, as evidenced by fewer and smaller metastatic nodules. These findings indicate that targeting circIL4R with shRNAs or siRNAs could effectively suppress CRC progression, highlighting its potential as a therapeutic target.

Mechanistically, bioinformatic analyses and subsequent validation experiments revealed that circIL4R promotes CRC malignancy through activation of the PI3K/AKT signaling pathway, which regulates multiple biological processes relevant to CRC progression [31]. For example, Xu *et al*. reported that lncRNA MALAT1 activates PI3K/AKT via the miR-26a/26b/FUT4 axis to enhance CRC proliferation and metastasis [50], while Kumar S *et al*. demonstrated that IDO1 promotes CRC cell proliferation and inhibits apoptosis via the PI3K/AKT pathway [51]. However, evidence linking circRNAs to PI3K/AKT activation in CRC has been limited.

Given that intracellular localization determines circRNA function, we examined circIL4R distribution and found it predominantly localized in the cytoplasm. Cytoplasmic circRNAs often regulate gene expression by acting as miRNA sponges [52]. Consistently, our study revealed that circIL4R sponges miR-761, confirmed through RNA pull-down, dual-luciferase reporter, and FISH assays. MiR-761 has been reported as a tumor suppressor that negatively regulates the PI3K/AKT pathway in several cancers [33, 34, 53, 54]. Our data showed that miR-761 suppresses CRC cell proliferation and metastasis, and its expression is reduced in CRC tissues and cell lines. Rescue experiments further confirmed that miR-761 antagonizes circIL4R's oncogenic effects and PI3K/AKT activation.

Besides functioning as competitive endogenous RNAs, circRNAs can encode peptides or interact with proteins [11, 55]. Analysis using circRNADb indicated that

circIL4R lacks an open reading frame, making protein translation unlikely. Nevertheless, catRAPID predictions suggested potential interactions with proteins such as SRSF9 and PTBP1, which are implicated in alternative splicing [56, 57]. Whether circIL4R modulates alternative splicing through these interactions requires further study.

Downstream, TRIM29 was identified as a target of miR-761 using four miRNA target prediction databases and TCGA/GEO data. Prior studies have linked miR-761 to TRIM29 regulation in other cancers, including triple-negative breast cancer [58]. In CRC, we confirmed the miR-761/TRIM29 interaction via qRT–PCR, western blot, and luciferase reporter assays. Functional rescue experiments demonstrated that TRIM29 overexpression reversed the inhibitory effects of circIL4R knockdown on PI3K/AKT signaling and CRC cell malignancy, indicating that the circIL4R/miR-761/TRIM29 axis drives CRC progression.

The precise mechanism by which TRIM29 activates PI3K/AKT remained unclear. TRIM29, a member of the tripartite motif family, has oncogenic roles in several cancers, including CRC, and has been reported to activate PI3K/AKT in thyroid cancer [22-24]. While PTEN, PHLPP1, and PP2A are established inhibitors of PI3K/AKT signaling [59], our data showed that TRIM29 manipulation did not alter PTEN or PP2A expression in CRC cells. Interestingly, TRIM29 knockdown increased PHLPP1 protein levels without affecting its mRNA, suggesting posttranscriptional regulation. Rescue experiments confirmed that PI3K/AKT inhibition due to TRIM29 knockdown was reversed by simultaneous PHLPP1 knockdown. Analogous to TRIM11-mediated PHLPP1 ubiquitination [41], we demonstrated that TRIM29 promotes PHLPP1 ubiquitination, leading to proteasomal degradation and subsequent PI3K/AKT activation. These findings indicate that TRIM29 activates PI3K/AKT via ubiquitin-mediated PHLPP1 degradation, although future studies should elucidate the specific domains involved.

Conclusion

In conclusion, our study identifies circIL4R as a novel circRNA upregulated in CRC tissues, cells, and serum, with potential diagnostic and prognostic value. We show that TFAP2C transcriptionally upregulates circIL4R, which functions as a miR-761 sponge to increase TRIM29 expression. TRIM29 subsequently targets PHLPP1 for ubiquitin-mediated degradation, leading to PI3K/AKT pathway activation and promoting CRC proliferation and metastasis **(Figure 9m)**. These findings provide new insights into CRC pathogenesis and suggest that circIL4R may serve as a promising target for diagnostic and therapeutic strategies in clinical practice.

Acknowledgments: We would like to thank Li Zhang for his assistance with the bioinformatics analysis and American Journal Exports for assistance with English language editing.

Conflict of Interest: None

Financial Support: Our study was funded by grants from the National Natural Science Foundation of China (82073133), the Scientific Research of Jiangsu Health Committee (ZDA2020005), the Natural Science Foundation of Jiangsu Province (BK20191154), and the ‘Six Talents Peak’ High-level Talent Project of Jiangsu Province (WSW-050), Xuzhou Medical Leading Talents Training Project (XWRCHT20210034).

Ethics Statement: None

References

1. Siegel RL, Miller KD, Fuchs HE, Jemal A. Cancer statistics, 2021. CA Cancer J Clin. 2021;71:7–33.
2. Provenzale D, Ness RM, Llor X, Weiss JM, Abbadessa B, Cooper G, et al. NCCN guidelines insights: colorectal cancer screening, version 2.2020. J Natl Compr Cancer Netw. 2020;18:1312–20.
3. Siegel RL, Miller KD, Goding Sauer A, Fedewa SA, Butterly LF, Anderson JC, et al. Colorectal cancer statistics, 2020. CA Cancer J Clin. 2020;70:145–64.
4. Kristensen LS, Andersen MS, Stagsted LVW, Ebbesen KK, Hansen TB, Kjems J. The biogenesis, biology and characterization of circular RNAs. Nat Rev Genet. 2019;20:675–91.
5. Shen T, Han M, Wei G, Ni T. An intriguing RNA species--perspectives of circularized RNA. Protein Cell. 2015;6:871–80.
6. Long F, Lin Z, Li L, Ma M, Lu Z, Jing L, et al. Comprehensive landscape and future perspectives of circular RNAs in colorectal cancer. Mol Cancer. 2021;20:26.

7. Geng Y, Jiang J, Wu C. Function and clinical significance of circRNAs in solid tumors. J Hematol Oncol. 2018;11:98.
8. Weng W, Wei Q, Toden S, Yoshida K, Nagasaka T, Fujiwara T, et al. Circular RNA ciRS-7-a promising prognostic biomarker and a potential therapeutic target in colorectal cancer. Clin Cancer Res. 2017;23:3918–28.
9. Chen RX, Chen X, Xia LP, Zhang JX, Pan ZZ, Ma XD, et al. N(6)-methyladenosine modification of circNSUN2 facilitates cytoplasmic export and stabilizes HMGA2 to promote colorectal liver metastasis. Nat Commun. 2019;10:4695.
10. Chen LY, Wang L, Ren YX, Pang Z, Liu Y, Sun XD, et al. The circular RNA circ-ERBIN promotes growth and metastasis of colorectal cancer by miR-125a-5p and miR-138-5p/4EBP-1 mediated cap-independent HIF-1alpha translation. Mol Cancer. 2020;19:164.
11. Chen LL. The expanding regulatory mechanisms and cellular functions of circular RNAs. Nat Rev Mol Cell Biol. 2020;21:475–90.
12. Zhong Y, Du Y, Yang X, Mo Y, Fan C, Xiong F, et al. Circular RNAs function as ceRNAs to regulate and control human cancer progression. Mol Cancer. 2018;17:79.
13. Tao M, Zheng M, Xu Y, Ma S, Zhang W, Ju S. CircRNAs and their regulatory roles in cancers. Mol Med. 2021;27:94.
14. Papatsirou M, Artemaki PI, Karousi P, Scorilas A, Kontos CK. Circular RNAs: emerging regulators of the major signaling pathways involved in cancer progression. Cancers (Basel). 2021;13:2744.
15. Farooqi AA, Naureen H, Attar R. Regulation of cell signaling pathways by circular RNAs and microRNAs in different cancers: spotlight on Wnt/beta-catenin, JAK/STAT, TGF/SMAD, SHH/GLI, NOTCH and hippo pathways. Semin Cell Dev Biol. 2021;S1084-9521:00075-6.
16. Zhang X, Yao J, Shi H, Gao B, Zhou H, Zhang Y, et al. Hsa_circ_0026628 promotes the development of colorectal cancer by targeting SP1 to activate the Wnt/beta-catenin pathway. Cell Death Dis. 2021;12:802.
17. Zheng X, Chen L, Zhou Y, Wang Q, Zheng Z, Xu B, et al. A novel protein encoded by a circular RNA circPPP1R12A promotes tumor pathogenesis and metastasis of colon cancer via hippo-YAP signaling. Mol Cancer. 2019;18:47.
18. Artemaki PI, Scorilas A, Kontos CK. Circular RNAs: a new piece in the colorectal cancer puzzle. Cancers (Basel). 2020;12:2464.
19. Sun J, Yan J, Qiao HY, Zhao FY, Li C, Jiang JY, et al. Loss of TRIM29 suppresses cancer stem cell-like characteristics of PDACs via accelerating ISG15 degradation. Oncogene. 2020;39:546–59.
20. Palmbos PL, Wang L, Yang H, Wang Y, Leflein J, Ahmet ML, et al. ATDC/TRIM29 drives invasive bladder cancer formation through miRNA-mediated and epigenetic mechanisms. Cancer Res. 2015;75:5155–66.
21. Wang L, Heidt DG, Lee CJ, Yang H, Logsdon CD, Zhang L, et al. Oncogenic function of ATDC in pancreatic cancer through Wnt pathway activation and beta-catenin stabilization. Cancer Cell. 2009;15:207–19.
22. Sun J, Zhang T, Cheng M, Hong L, Zhang C, Xie M, et al. TRIM29 facilitates the epithelial-to-mesenchymal transition and the progression of colorectal cancer via the activation of the Wnt/beta-catenin signaling pathway. J Exp Clin Cancer Res. 2019;38:104.
23. Han J, Zhao Z, Zhang N, Yang Y, Ma L, Feng L, et al. Transcriptional dysregulation of TRIM29 promotes colorectal cancer carcinogenesis via pyruvate kinase-mediated glucose metabolism. Aging (Albany NY). 2021;13:5034–54.
24. Xu J, Li Z, Su Q, Zhao J, Ma J. TRIM29 promotes progression of thyroid carcinoma via activating P13K/AKT signaling pathway. Oncol Rep. 2017;37:1555–64.
25. Hou P, Shi P, Jiang T, Yin H, Chu S, Shi M, et al. DKC1 enhances angiogenesis by promoting HIF-1alpha transcription and facilitates metastasis in colorectal cancer. Br J Cancer. 2020;122:668–79.
26. Zheng X, Huang M, Xing L, Yang R, Wang X, Jiang R, et al. The circRNA circSEPT9 mediated by E2F1 and EIF4A3 facilitates the carcinogenesis and development of triple-negative breast cancer. Mol Cancer. 2020;19:73.
27. Meng J, Chen S, Han JX, Qian B, Wang XR, Zhong WL, et al. Twist1 regulates Vimentin through Cul2 circular RNA to promote EMT in hepatocellular carcinoma. Cancer Res. 2018;78:4150–62.
28. Wang X, Sun D, Tai J, Chen S, Yu M, Ren D, et al. TFAP2C promotes stemness and chemotherapeutic resistance in colorectal cancer via inactivating hippo

signaling pathway. J Exp Clin Cancer Res. 2018;37:27.
29. Yang P, Li J, Peng C, Tan Y, Chen R, Peng W, et al. TCONS_00012883 promotes proliferation and metastasis via DDX3/YY1/MMP1/PI3K-AKT axis in colorectal cancer. Clin Transl Med. 2020;10:e211.
30. Han Y, Peng Y, Fu Y, Cai C, Guo C, Liu S, et al. MLH1 deficiency induces Cetuximab resistance in colon cancer via Her-2/PI3K/AKT signaling. Adv Sci (Weinh). 2020;7:2000112.
31. Koveitypour Z, Panahi F, Vakilian M, Peymani M, Seyed Forootan F, Nasr Esfahani MH, et al. Signaling pathways involved in colorectal cancer progression. Cell Biosci. 2019;9:97.
32. Xu Q, Zhou L, Yang G, Meng F, Wan Y, Wang L, et al. CircIL4R facilitates the tumorigenesis and inhibits ferroptosis in hepatocellular carcinoma by regulating the miR-541-3p/GPX4 axis. Cell Biol Int. 2020;44:2344–56.
33. Zhi Q, Wan D, Ren R, Xu Z, Guo X, Han Y, et al. Circular RNA profiling identifies circ102049 as a key regulator of colorectal liver metastasis. Mol Oncol. 2021;15:623–41.
34. Lv Z, Ma J, Wang J, Lu J. MicroRNA-761 targets FGFR1 to suppress the malignancy of osteosarcoma by deactivating PI3K/Akt pathway. Onco Targets Ther. 2019;12:8501–13.
35. Zhou XM, Sun R, Luo DH, Sun J, Zhang MY, Wang MH, et al. Upregulated TRIM29 promotes proliferation and metastasis of nasopharyngeal carcinoma via PTEN/AKT/mTOR signal pathway. Oncotarget. 2016;7:13634–50.
36. Zhang M, Wang X, Liu M, Liu D, Pan J, Tian J, et al. Inhibition of PHLPP1 ameliorates cardiac dysfunction via activation of the PI3K/Akt/mTOR signalling pathway in diabetic cardiomyopathy. J Cell Mol Med. 2020;24:4612–23.
37. Salvatore L, Calegari MA, Loupakis F, Fassan M, Di Stefano B, Bensi M, et al. PTEN in colorectal cancer: shedding light on its role as predictor and target. Cancers (Basel). 2019;11:1765.
38. Patel R, Gao M, Ahmad I, Fleming J, Singh LB, Rai TS, et al. Sprouty2, PTEN, and PP2A interact to regulate prostate cancer progression. J Clin Invest. 2013;123:1157–75.
39. Zheng X, Yu S, Xue Y, Yan F. FBXO22, ubiquitination degradation of PHLPP1, ameliorates rotenone induced neurotoxicity by activating AKT pathway. Toxicol Lett. 2021;350:1–9.
40. Zhang CX, Huang DJ, Baloche V, Zhang L, Xu JX, Li BW, et al. Galectin-9 promotes a suppressive microenvironment in human cancer by enhancing STING degradation. Oncogenesis. 2020;9:65.
41. Wang B, Wang G, Wang Q, Zhu Z, Wang Y, Chen K, et al. Silencing of TRIM11 suppresses the tumorigenicity of chordoma cells through improving the activity of PHLPP1/AKT. Cancer Cell Int. 2019;19:284.
42. Zhang M, Xin Y. Circular RNAs: a new frontier for cancer diagnosis and therapy. J Hematol Oncol. 2018;11:21.
43. Sole C, Arnaiz E, Manterola L, Otaegui D, Lawrie CH. The circulating transcriptome as a source of cancer liquid biopsy biomarkers. Semin Cancer Biol. 2019;58:100–8.
44. Han B, Chao J, Yao H. Circular RNA and its mechanisms in disease: from the bench to the clinic. Pharmacol Ther. 2018;187:31–44.
45. Wen G, Zhou T, Gu W. The potential of using blood circular RNA as liquid biopsy biomarker for human diseases. Protein Cell. 2020. https://doi.org/10.1007/s13238-020-00799-3.
46. Gu Z, Zhou Y, Cao C, Wang X, Wu L, Ye Z. TFAP2C-mediated LINC00922 signaling underpins doxorubicin-resistant osteosarcoma. Biomed Pharmacother. 2020;129:110363.
47. Chen J, Liu X, Xu Y, Zhang K, Huang J, Pan B, et al. TFAP2C-activated MALAT1 modulates the Chemoresistance of Docetaxel-resistant lung adenocarcinoma cells. Mol Ther Nucleic Acids. 2019;14:567–82.
48. Wei Y, Lu C, Zhou P, Zhao L, Lyu X, Yin J, et al. EIF4A3-induced circular RNA ASAP1 promotes tumorigenesis and temozolomide resistance of glioblastoma via NRAS/MEK1/ERK1-2 signaling. Neuro-Oncology. 2021;23:611–24.
49. Errichelli L, Dini Modigliani S, Laneve P, Colantoni A, Legnini I, Capauto D, et al. FUS affects circular RNA expression in murine embryonic stem cell-derived motor neurons. Nat Commun. 2017;8:14741.
50. Xu J, Xiao Y, Liu B, Pan S, Liu Q, Shan Y, et al. Exosomal MALAT1 sponges miR-26a/26b to promote the invasion and metastasis of colorectal cancer via FUT4 enhanced fucosylation and PI3K/Akt pathway. J Exp Clin Cancer Res. 2020;39:54.

51. Bishnupuri KS, Alvarado DM, Khouri AN, Shabsovich M, Chen B, Dieckgraefe BK, et al. IDO1 and Kynurenine pathway metabolites activate PI3K-Akt signaling in the neoplastic colon epithelium to promote cancer cell proliferation and inhibit apoptosis. Cancer Res. 2019;79:1138–50.
52. Tay Y, Rinn J, Pandolfi PP. The multilayered complexity of ceRNA crosstalk and competition. Nature. 2014;505:344–52.
53. Wang X, Li C, Yao W, Tian Z, Liu Z, Ge H. MicroRNA-761 suppresses tumor progression in osteosarcoma via negatively regulating ALDH1B1. Life Sci. 2020;262:118544.
54. Li C, Zhou H. Circular RNA hsa_circRNA_102209 promotes the growth and metastasis of colorectal cancer through miR-761-mediated Ras and Rab interactor 1 signaling. Cancer Med. 2020;9:6710–25.
55. Wang J, Zhu S, Meng N, He Y, Lu R, Yan GR. ncRNA-encoded peptides or proteins and cancer. Mol Ther. 2019;27:1718–25.
56. Campagne S, de Vries T, Malard F, Afanasyev P, Dorn G, Dedic E, et al. An in vitro reconstituted U1 snRNP allows the study of the disordered regions of the particle and the interactions with proteins and ligands. Nucleic Acids Res. 2021;49:e63.
57. Oh J, Liu Y, Choi N, Ha J, Pradella D, Ghigna C, et al. Opposite roles of Tra2beta and SRSF9 in the v10 exon splicing of CD44. Cancers (Basel). 2020;12:3195.
58. Guo GC, Wang JX, Han ML, Zhang LP, Li L. microRNA-761 induces aggressive phenotypes in triple-negative breast cancer cells by repressing TRIM29 expression. Cell Oncol (Dordr). 2017;40:157–66.
59. Chen M, Nowak DG, Trotman LC. Molecular pathways: PI3K pathway phosphatases as biomarkers for cancer prognosis and therapy. Clin Cancer Res. 2014;20:3057–63.